






Research article

[urn:lsid:zoobank.org/pub:CBC9DA40-EC6D-4280-8BBC-6826D72A291E](https://zoobank.org/pub:CBC9DA40-EC6D-4280-8BBC-6826D72A291E)

**Delimitation of *Ophioderma teres* (Lyman, 1860) and
Ophioderma unicolor H.L. Clark, 1940 stat. nov.
(Echinodermata: Ophiuroidea),
including the description of two new species**

Karla J. HUMARA-GIL ¹, Rebeca GRANJA-FERNÁNDEZ ²,
Eric BAUTISTA-GUERRERO ³, Francisco A. SOLÍS-MARÍN ⁴ &
Alma P. RODRÍGUEZ-TRONCOSO ^{5,*}

^{1,3,5}Laboratorio de Ecología Marina, Centro Universitario de la Costa, Universidad de Guadalajara, Puerto Vallarta, Mexico.

²Postdoctoral researcher (CONAHCYT) associated with Programa de Maestría en Biosistemática y Manejo de Recursos Naturales y Agrícolas (BIMARENA) / Laboratorio de Ecología Molecular, Microbiología y Taxonomía (LEMITAX). Centro Universitario de Ciencias Biológicas y Agropecuarias, Universidad de Guadalajara, Zapopan, Mexico.

⁴Colección Nacional de Equinodermos “Dra. Ma. Elena Caso Muñoz”, Laboratorio de Sistemática y Ecología de Equinodermos, Instituto de Ciencias del Mar y Limnología (ICML), Universidad Nacional Autónoma de México (UNAM), Mexico City, Mexico.

* Corresponding author: alma.rtroncoso@academicos.udg.mx

¹ Email: k.humaragil@gmail.com

² Email: beckygranja@gmail.com

³ Email: eric.bautista0177@academicos.udg.mx

⁴ Email: fasolis@cmarl.unam.mx

¹ [urn:lsid:zoobank.org:author:8173990E-CA82-4B7C-BE3E-D31228CB51CD](https://zoobank.org/urn:lsid:zoobank.org:author:8173990E-CA82-4B7C-BE3E-D31228CB51CD)

² [urn:lsid:zoobank.org:author:98B31C6C-C2FF-4BC2-A556-5782D3001A91](https://zoobank.org/urn:lsid:zoobank.org:author:98B31C6C-C2FF-4BC2-A556-5782D3001A91)

³ [urn:lsid:zoobank.org:author:0C7DC2DA-EBB9-4998-9237-F7C7FC86B96F](https://zoobank.org/urn:lsid:zoobank.org:author:0C7DC2DA-EBB9-4998-9237-F7C7FC86B96F)

⁴ [urn:lsid:zoobank.org:author:A2417F0D-CA2A-4BE2-A6F0-C8991F4B90EA](https://zoobank.org/urn:lsid:zoobank.org:author:A2417F0D-CA2A-4BE2-A6F0-C8991F4B90EA)

⁵ [urn:lsid:zoobank.org:author:B44F0417-F061-4B52-8AE6-190149FA2E41](https://zoobank.org/urn:lsid:zoobank.org:author:B44F0417-F061-4B52-8AE6-190149FA2E41)

Abstract. *Ophioderma teres* (Lyman, 1860), an ophiuroid previously believed to have a wide distribution in the eastern Pacific, has been found to have an unclear taxonomic identity. While considered a well-known species, recent studies have revealed that *O. teres* lacks a holotype and has vague boundaries with its congeners *Ophioderma teres unicolor* H.L. Clark, 1940 and *Ophioderma sodipallaresi* Caso, 1986, as well as with two additional new morphotypes detected in Mexico and Nicaragua, causing continuous misidentifications. This study utilized an integrative taxonomy approach based on morphologic, morphometric, and molecular evidence to clarify the taxonomic status of *O. teres*, *O. sodipallaresi*, *O. teres unicolor*, and the two new morphotypes. Data integration led to the following results: 1) the neotype designation and redescription of *O. teres*; 2) the proposal of *O. sodipallaresi* as a junior synonym of *O. teres*; 3) the status change of *O. unicolor* stat. nov. from subspecies to species, and 4) the

description of the morphotypes as the new species *Ophioderma aija* sp. nov. and *Ophioderma bichi* sp. nov. An identification key to the eastern Pacific species of *Ophioderma* was also developed. This work contributes to the knowledge of *Ophioderma* in the region, increasing the number of described species and providing resources for their accurate identification.

Keywords. 16S, brittle stars, COI, integrative taxonomy, neotype.

Humara-Gil K.J., Granja-Fernández R., Bautista-Guerrero E., Solís-Marín F.A. & Rodríguez-Troncoso A.P. 2024. Delimitation of *Ophioderma teres* (Lyman, 1860) and *Ophioderma unicolor* H.L. Clark, 1940 stat. nov. (Echinodermata: Ophiuroidea), including the description of two new species. *European Journal of Taxonomy* 947: 130–174. <https://doi.org/10.5852/ejt.2024.947.2625>

Introduction

Along with *Ophioderma variegatum* Lütken, 1856 and *Ophioderma panamense* Lütken, 1859, *Ophioderma teres* (Lyman, 1860) is one of the earliest known ophiidermatid brittle stars from the eastern Pacific (EP). This species, originally classified under the genus *Ophiura* Lamarck, 1801, was described by Theodore Lyman in 1860, based on a Panamanian specimen (Lyman 1860). Since then, it has been reported from the southwestern United States of America (USA) to Peru (Maluf 1988; Granja-Fernández & Hooker 2020), being the second most frequently documented *Ophioderma* in the region after *O. panamense* (Solís-Marín *et al.* 2013).

In 1940, Hubert Lyman Clark examined the echinoderms collected during the 1937–1938 EP Zaca expedition and, among his findings, proposed a variety of *O. teres*; he named it “*unicolor*” because of its uniform dark brown coloration, in contrast to the speckled appearance of *O. teres* (Lyman 1860; H.L. Clark 1940). The former variety is currently known as the subspecies *Ophioderma teres unicolor* H.L. Clark, 1940 (ICZN 1999; Humara-Gil *et al.* 2022). The original description of *O. teres unicolor* is unclear as it solely mentions its coloration (H.L. Clark 1940). This vagueness has hindered its identification, leading to doubts about its validity (Ziesenhenné 1955). The subspecies has an uncertain taxonomic status and is categorized as a taxon inquirendum in the World Ophiuroidea Database (Stöhr *et al.* 2023a).

During recent visits to various scientific collections, type and non-type material of *O. teres* and *O. teres unicolor* was searched to compare them and clarify the latter’s status. However, the examination revealed further issues. First, the holotype of *O. teres* could not be located, and second, distinct morphotypes were recognized among the specimens identified as *O. teres* and *O. teres unicolor*. The lack of type material, the numerous misidentifications, and the discovery of potentially new similar species evidenced that not only was it necessary to elucidate the taxonomic status of *O. teres unicolor* but also to delimit *O. teres*. Moreover, examination of the type material of EP *Ophioderma* revealed an additional nominal species with a highly similar morphology to *O. teres*, *Ophioderma sodipallaresi* Caso, 1986, described from Pájaros Island in Mazatlán, Mexico (Caso 1986). The remarkable resemblance between the two may suggest that they belong to the same species.

This study aimed to resolve the taxonomic status of *O. teres*, its relatives *O. sodipallaresi* and *O. teres unicolor*, as well as the new morphotypes identified (hereinafter *Ophioderma* sp. A and *Ophioderma* sp. B). The above was carried out through an integrative analysis that included morphological (external and internal), morphometric, and molecular (cytochrome c oxidase subunit I (COI) and 16S rRNA (16S)) data, depending on the availability of the material. The current work contributes to the knowledge of the genus *Ophioderma* in the EP region by increasing the number of described species and providing

resources (i.e., descriptions, figures, DNA barcodes, and an identification key) for the accurate taxonomic determination of its commonly misidentified representatives.

Material and methods

Type and non-type specimens (when applicable) of *O. sodipallaresi* (n = 6), *O. teres* (n = 43), *O. teres unicolor* (n = 7), *Ophioderma* sp. A (n = 94), and *Ophioderma* sp. B (n = 49) from scientific collections were thoroughly examined. The type material of the remaining EP *Ophioderma*, including *O. hendleri* Granja-Fernández *et al.*, 2020, *O. occultum* Humara-Gil *et al.*, 2022, *O. panamense*, *O. pentacanthum* H.L. Clark, 1917, *O. peruanum* Pineda-Enríquez *et al.*, 2013, *O. vansyoci* Hendler, 1996, and *O. variegatum*, was also examined for comparative purposes. Additional material of *Ophioderma* sp. A (n = 48) and *Ophioderma* sp. B (n = 7) (originally identified as *O. teres* or *O. teres unicolor*) was collected from 2011 to 2020 along the Mexican Pacific coast. The specimens were anesthetized using a menthol/seawater solution or exposed to low temperatures (5–10°C) for one hour to prevent arm autotomy during fixation. Then, they were fixed and preserved in 70% or 96% ethanol or air-dried and examined. All specimens are listed either in the Material examined sections of each species or in the Supplementary material ([Supp. file 1](#), [Supp. file 2](#)) and are deposited in the following scientific collections:

CE-UAM	=	Colección de Equinodermos, Universidad Autónoma Metropolitana-Iztapalapa, Mexico City, Mexico
CZA	=	Colección de Zoología Acuática, Universidad Peruana Cayetano Heredia, Lima, Peru
ICML-EMU	=	Colección Regional de Invertebrados Marinos, Unidad Académica Mazatlán, Universidad Nacional Autónoma de México, Mazatlán, Sinaloa, Mexico
ICML-UNAM	=	Colección Nacional de Equinodermos “Dra. Ma. Elena Caso Muñoz”, Instituto de Ciencias del Mar y Limnología, Universidad Nacional Autónoma de México, Mexico City, Mexico
LACM	=	Natural History Museum of Los Angeles County, Los Angeles, USA
MCZ	=	Museum of Comparative Zoology, Harvard University, Cambridge, USA
MZUCR	=	Museo de Zoología, Universidad de Costa Rica, San José, Costa Rica
NHMD	=	Natural History Museum of Denmark, University of Copenhagen, Copenhagen, Denmark
UMML	=	Voss Marine Invertebrate Collection, Rosenstiel School of Marine, Atmospheric and Earth Science, University of Miami, Miami, USA
USNM	=	Smithsonian National Museum of Natural History, Washington DC, USA

The specimens were examined using a stereo microscope and photographed with an adapted Canon EOS Rebel T8i camera. Specimens of equivalent size (disc diameter (DD) = ~26–28 mm) of *O. teres* (n = 2), *Ophioderma* sp. A (n = 2), and *Ophioderma* sp. B (n = 2) were selected for scanning electron microscopy (SEM); *O. sodipallaresi* and *O. teres unicolor* were excluded due to the limited number of available specimens (n = 6 and 7, respectively). One-fifth of the disc and the proximalmost arm section of the longest arm were dissected from each specimen and treated with undiluted household bleach (NaClO) to dissolve the integument. Disarticulated ossicles were washed three times with distilled water and once with 96% ethanol. After drying, the ossicles were mounted on aluminum stubs with double-sided adhesive carbon tabs, maintained in a desiccator for 24 hours, and coated with gold-palladium or gold. The samples were photographed using a Zeiss EVO MA 15 at USNM and a Hitachi SU1510 at the Laboratorio de Microscopía y Fotografía de la Biodiversidad I, Instituto de Biología, Universidad Nacional Autónoma de México, Mexico City, Mexico (IBUNAM).

For the morphometric analysis, measurements and counts were obtained from intact, well-preserved animals of *O. hendleri* (n = 22), *O. occultum* (n = 17), *O. panamense* (n = 24), *O. sodipallaresi* (n = 6),

O. teres (n = 14), *O. teres unicolor* (n = 3), *Ophioderma* sp. A (n = 15), and *Ophioderma* sp. B (n = 16) with DD = 9.9–20.9 mm, the size range of the species with the least available material (*O. sodipallaresi*), so that the data were comparable between species/morphotypes. The variables were the following: 1) disc: DD; 2) jaws: oral shield width and length (the first to the right of the madreporite), jaw length (the first to the right of the madreporite), number of lateral oral papillae (LOPs); 3) arms: length of the longest arm (AL), number of pieces conforming the dorsal arm plates (DAPs) (three segments from the proximal and median arm sections), first ventral arm plate (1VAP) width and length, VAP width and length (median arm section), adradial tentacle scale length (median arm section), number of arm spines (three segments from the proximal arm section and one from the median arm section), and number of arm segments with pores present between the proximalmost VAPs. Methodological specifications and an illustrated account of the measurements are given in [Supp. file 3](#). DD and AL, as well as measurements obtained from the same structure (oral shield width and length, 1VAP width and length, VAP width and length), were assessed as ratios. To avoid redundant data, the variables were evaluated with a correlation matrix, and those with correlation coefficients of 0.9 or higher were excluded from further analyses (see [Supp. file 4](#)).

A one-way permutational multivariate analysis of variance (PERMANOVA) (Anderson 2001) with 9999 permutations based on a Euclidean distance matrix was performed to test for differences in morphometric data between species/morphotypes (function “adonis2”, package “vegan”) (Oksanen *et al.* 2022). To explore differences, pairwise comparisons applying the Bonferroni correction were conducted (function “pairwise.adonis2”, package “pairwiseAdonis”) (Martinez-Arbizu 2017). Lastly, a similarity percentages analysis (SIMPER) (Clarke 1993) was used to determine the contribution of morphometric variables to the dissimilarity between species/morphotypes. The analyses were performed in R ver. 4.3.1 (PERMANOVA, pairwise comparisons) (R Core Team 2023) and Past ver. 4.3 (SIMPER) (Hammer *et al.* 2021).

Specimens of *O. hendleri* (n = 3), *O. occultum* (n = 3), *O. panamense* (n = 3), *Ophioderma* sp. A (n = 3), and *Ophioderma* sp. B (n = 2) collected in the Mexican Pacific were used for DNA analysis. DNA extraction, amplification, sequencing, and editing adhered to the procedures described in Humara-Gil *et al.* (2022). Partial COI sequences (> 500 bp) were obtained using the primer set OphCOI-For (5'-CAA CAY YTA TTY TGR TTY TTY GG-3') and OphCOI-Rev (5'-CCT ARR AAR TGT TGW GGG AAR AA-3') (Lessios & Hendler 2022). For 16S partial sequences (< 500 bp), the primer set used was 16SAR (5'-CGC CTG TTT ATC AAA AAC AT-3') and 16SBR (5'-CCG GTC TGA ACT CAG ATC ACG T-3') (Palumbi 1996). Thermal cycling conditions were: 1) 2 min at 95°C; 2) 35 cycles of 50 s at 95°C, 50 s at 48.5°C, 1 min at 72°C (COI) or 41 cycles of 30 s at 95°C, 40 s at 48°C, 1 min at 72°C (16S); and 3) 10 min at 72°C. The sequences generated in this study are available in GenBank (see [Supp. file 5](#)).

Additional COI sequences of *O. hendleri*, *O. panamense*, *O. teres*, and *O. variegatum* (576–1419 bp) from El Salvador, Costa Rica, and Panama, as well as 16S sequences of *O. hendleri*, *O. occultum*, *O. panamense*, and *Ophioderma* sp. A (recorded as *Ophioderma* cf. *teres unicolor*) (493–500 bp) from Mexico were also included in the analyses. Sequences of *Ophiopeza spinosa* (Ljungman, 1867) and *Ophiopeza fallax* Peters, 1851 were used as outgroups on COI and 16S trees, respectively. These were all retrieved from GenBank from previous works (Hoareau *et al.* 2013; Hugall *et al.* 2016; Humara-Gil *et al.* 2022; Lessios & Hendler 2022) (see [Supp. file 5](#)).

The COI and 16S datasets were analyzed separately. Sequences were aligned using the MUSCLE algorithm (Edgar 2004) and cut in MEGA ver. 11.0.13 (Tamura *et al.* 2021). The best-fitting substitution models were obtained in jModelTest ver. 2.1.10 (Darriba *et al.* 2012) based on the Akaike and Bayesian Information Criteria scores: General Time Reversible model + gamma distributed rates with invariant sites (GTR + G + I) for COI, and General Time Reversible model + invariant sites (GTR + I) for 16S.

Maximum likelihood (ML) trees were built in MEGA ver. 11.0.13, applying 1000 bootstrap replicates and the corresponding substitution model. Bayesian inference (BI) trees were obtained with MrBayes ver. 3.2.6 (Ronquist *et al.* 2012). The Markov chain Monte Carlo (MCMC) analysis was run with four chains for 160 000 generations, after which the average standard deviation of the split frequencies reached a value below 0.01. One tree was sampled every 100 generations, discarding the initial 25% as burn-in. A consensus tree based on the remaining sampled trees was then obtained. Genetic distances between species/morphotypes were estimated by p-distances in MEGA ver. 11.0.13.

The resulting BI trees were also analyzed using the Bayesian Poisson tree processes (bPTP) for species delimitation (Zhang *et al.* 2013). This was conducted through the bPTP web server: species.h-its.org/ptp/. Analyses were run for 100 000 generations, with a thinning of 100 and a burn-in of 25%.

Available morphological (external and internal), morphometric, and molecular (COI and 16S) data were integrated to validate the taxonomic status of each species/morphotype, following the consensus protocol for integrative taxonomy of Padial *et al.* (2010). This protocol merges integration by cumulation (i.e., differences in any source of evidence may indicate that a species is distinct) and integration by congruence (i.e., concordant differences in two or more sources of evidence indicate that a species is distinct) to delimit species, combining their advantages (Padial *et al.* 2010).

Finally, in the systematic account, synonymy lists include the original name and reference to the original description, junior synonyms (if any), studies that unequivocally recorded or described the species, and those where the species was misidentified. When the records of the species were not supported by voucher specimens or the species' identity could not be verified, the reference was omitted. Morphological terminology follows Stöhr *et al.* (2012), Thuy & Stöhr (2016), and Hendler (2018); systematics follows O'Hara *et al.* (2018).

Abbreviations

2°AdShSp	=	secondary adoral shield spine
AdShSp	=	adoral shield spine
IPa	=	infradental papilla
LAP	=	lateral arm plate
LyOs	=	Lyman's ossicle
OPRSp	=	oral plate ridge spine
spec.	=	specimen
TPa	=	tooth papillae
vT	=	ventralmost tooth

Results

External and internal morphology

The examination of *O. sodipallaresi*, *O. teres*, *O. teres unicolor*, *Ophioderma* sp. A, and *Ophioderma* sp. B revealed differences in their external morphology, mainly in the AL:DD ratio, state of the radial shields (covered with granules or naked), distal genital slit ornamentation, number of DAP pieces, maximum number of arm spines, and color pattern (Table 1).

Regarding internal morphology, the main differences between the species/morphotypes from which the ossicles were obtained, *O. teres*, *Ophioderma* sp. A, and *Ophioderma* sp. B, were detected in the radial shields and oral plates. The radial shields of *Ophioderma* sp. A presented a raised oval-shaped section in the center with no pores, corresponding to the naked part of the shield observed in the intact animal. On the other hand, the radial shields of *O. teres* and *Ophioderma* sp. B were more regular and did have

Table 1. Main external and internal morphological characters that distinguish the studied species/morphotypes of *Ophioderma* Müller & Troschel, 1840. The number of DAP pieces is given as an interval, followed by the mean in parentheses. A dash (–) indicates no data are available due to lack of material. Abbreviations: AL = arm length; DAP = dorsal arm plate; DD = disc diameter.

Species/morphotype	<i>O. sodipallaresi</i>	<i>O. teres</i>	<i>O. teres unicolor</i>	<i>Ophioderma</i> sp. A	<i>Ophioderma</i> sp. B
External morphology					
Morphological character	n = 6 9.9–20.9 mm DD	n = 43 11.6–33.8 mm DD	n = 7 17.1–35.7 mm DD	n = 142 6.5–26.7 mm DD	n = 56 9.1–33.2 mm DD
AL:DD ratio	3.4	3.4	3.4	2.7	3.7
Radial shields	covered/naked	covered/naked	naked	naked	covered
Distal genital slit ornamentation	granule-bearing scales	naked and granule-bearing scales	naked and granule-bearing scales	naked and granule-bearing scales	granule-bearing scales
No. of DAP pieces	1–5 (2)	1–13 (3)	1–6 (2)	1–9 (3)	1–9 (2)
Maximum no. of arm spines	10	12	13	10	12
Color pattern	brown speckled with cream	brown speckled with cream	uniform brown	dark brown with darker, sinuous rings on the disc	uniform brown
Internal morphology					
Radial shields	–	n = 2 26.9–27.8 mm DD distal half with a swollen center and scattered pores	–	n = 2 26.2–26.4 mm DD distal half with a central raised oval-shaped section without pores	n = 2 28.0–28.1 mm DD distal half with a swollen center and scattered pores
Oral plates	–	robust, compact	–	lower, elongated	robust, compact

Table 2. Morphometric data with the highest contribution to the differentiation of the studied species/morphotypes of *Ophioderma* Müller & Troschel, 1840. The ratios and counts are indicated as intervals, followed by the mean in parentheses. Abbreviations: 1VAP_W:L = first ventral arm plate (VAP) width:length ratio; AS_prox_3_5 = number of arm spines in the 3rd or 5th proximal arm segment; DAPs_med_1_2_3 = number of DAP pieces in the 1st, 2nd or 3rd median arm segment; DAPs_prox_3_4_5 = number of dorsal arm plate (DAP) pieces in the 3rd, 4th or 5th proximal arm segment; DD = disc diameter; LOPas = lateral oral papillae; OSh_W:L = oral shield width:length ratio; VAP_L:W_med = VAP length:width ratio (median arm section); VAP_pores = number of arm segments with pores present between the proximalmost VAPs.

Species/morphotype	<i>O. sodipallaresi</i>	<i>O. teres</i>	<i>O. teres unicolor</i>	<i>Ophioderma</i> sp. A	<i>Ophioderma</i> sp. B
Morphometric character	n = 6	n = 14	n = 3	n = 15	n = 56
	9.9–20.9 mm DD	11.6–20.4 mm DD	17.1–20.7 mm DD	10.6–19.9 mm DD	10.3–19.5 mm DD
Jaws					
OSh_W:L	1.0–1.4 (1.2)	1.3–1.7 (1.4)	1.4–1.7 (1.5)	1.2–1.7 (1.4)	1.1–1.7 (1.3)
LOPas	4–6 (5)	3–6 (5)	4–7 (5)	3–6 (5)	3–5 (4)
Arms					
DAPs_prox_3	1–3 (2)	1–5 (3)	1–2 (2)	2–6 (4)	1–4 (2)
DAPs_prox_4	1–4 (2)	1–6 (3)	1–2 (1)	1–6 (3)	1–3 (2)
DAPs_prox_5	1–5 (3)	1–7 (3)	1–2 (2)	2–5 (3)	1–6 (2)
DAPs_med_1	1–3 (2)	1–5 (2)	1–2 (1)	1–4 (2)	1–2 (1)
DAPs_med_2	1–3 (2)	1–3 (2)	1–2 (1)	1–5 (3)	1–2 (1)
DAPs_med_3	1–2 (2)	1–4 (2)	1–2 (1)	2–4 (2)	1–2 (1)
1VAP_W:L	1.6–2.2 (1.9)	1.5–3.1 (1.9)	1.6–1.8 (1.7)	1.5–2.9 (1.9)	1.3–2.3 (1.7)
VAP_L:W_med	1.0–1.5 (1.2)	0.9–1.7 (1.2)	1.0–1.1 (1.1)	0.8–1.8 (1.2)	1.0–1.4 (1.2)
AS_prox_3	7–10 (8)	7–9 (8)	9–12 (10)	7–9 (8)	7–10 (8)
AS_prox_5	7–10 (9)	7–9 (8)	10–12 (11)	6–9 (8)	6–10 (8)
VAP_pores	1–2 (2)	0–2 (1)	1–2 (1)	1–3 (2)	0–2 (1)

pores scattered on the surface. The second difference was observed in the oral plates. *Ophioderma teres* and *Ophioderma* sp. B had oral plates proportionally more robust and compact than *Ophioderma* sp. A, which showed lower and elongated oral plates, particularly in the middle section (Table 1).

Morphometric analyses

The PERMANOVA revealed significant differences in the morphometric data between species/morphotypes ($F_{7,116} = 7.179, p = 0.0001$). Pairwise comparisons indicated that most species/morphotypes were significantly different from each other, except for *O. sodipallaresi* versus *O. teres* ($p = 0.335$), *O. teres unicolor* ($p = 0.0696$), and *Ophioderma* sp. B ($p = 0.2642$), respectively, and *O. teres* versus *Ophioderma* sp. A ($p = 0.3997$) (see [Supp. file 6](#)).

SIMPER analysis indicated that, considering all the species/morphotypes analyzed, average dissimilarities between significantly different species/morphotypes were mainly attributed to variables such as AL:DD, the number of LOPas, median VAP length:width, 1VAP width:length, the number of DAP pieces on the 5th proximal arm segment, and the number of arm spines of the 3rd and 5th proximal arm segments, with contributions between 9.2% and 24.2%. In contrast, the variables that least influenced the dissimilarities were the jaw length, the number of DAP pieces on the 3rd and 4th segments of the proximalmost arm section and on the three segments of the median arm section, and the adradial tentacle scale length, with contributions of 0–3.3%. Dissimilarity values ranged from 10.96% between *O. hendleri* and *O. panamense* to 33.91% between *O. hendleri* and *Ophioderma* sp. A (see [Supp. file 6](#)).

Specifically for the *O. teres*-like group, the most important variables that cumulatively contributed up to 50% to the dissimilarities between species were the oral shield width:length, the number of LOPas, the number of DAP pieces on the 3rd, 4th, and 5th proximal arm segments and in the 1st, 2nd, and 3rd median arm segment, 1VAP width:length, median VAP width:length, and the number of arm segments with pores between the proximalmost VAPs (Table 2) (see [Supp. file 6](#)).

Molecular analyses

In the COI analyses, 531 bp were considered. Of the analyzed sites, 339 (63.8%) were conserved and 192 (36.2%) were variable, with 147 (27.7%) being parsimony informative. In the case of 16S, 446 bp were analyzed. Of these, 325 (72.9%) sites were conserved and 121 (27.1%) were variable, 113 (25.3%) of which were parsimony informative.

The COI tree showed a main clade grouping the EP *Ophioderma*, divided in turn into two subclades. The first subclade included *O. hendleri*, *O. occultum*, *O. panamense*, and *O. variegatum* (posterior probability = 0.64). The three latter species formed a secondary subclade (posterior probability = 0.98; bootstrap value = 61), with *O. occultum* and *O. panamense* recovered as sister species (posterior probability = 1.0; bootstrap value = 100). The second subclade contained *O. teres*, *Ophioderma* sp. A, and *Ophioderma* sp. B (posterior probability = 0.82; bootstrap value = 97). In this subclade, *Ophioderma* sp. A was recovered as the sister of *O. teres* (posterior probability = 1.0; bootstrap value = 100) (Fig. 1).

The 16S tree also showed the main EP *Ophioderma* clade. Within this clade, *O. hendleri* was separated from a subclade including *O. occultum*, *O. panamense*, *Ophioderma* sp. A, and *Ophioderma* sp. B (posterior probability = 0.85; bootstrap value = 68). In this last subclade, *O. occultum* and *O. panamense* (posterior probability = 1.0; bootstrap value = 99), as well as *Ophioderma* sp. A and *Ophioderma* sp. B, but with lower support (posterior probability = 0.85; bootstrap value = 69), were recovered as sisters (Fig. 2). Remarkably, COI and 16S topologies, with both BI and ML, retrieved the two morphotypes, *Ophioderma* sp. A and *Ophioderma* sp. B, in separate highly supported clades (posterior probabilities = 0.86–1.0; bootstrap values = 99–100) (Figs 1–2).

The mean genetic distances estimated for COI ranged from 3.3% (*O. teres* and *Ophioderma* sp. A) to 13.2% (*O. hendleri* and *O. panamense*) among *Ophioderma* and up to 21.7% (*O. panamense* and *O. spinosa*) considering the outgroup *Ophiopeza*. As for 16S, genetic distances ranged from 3.0% (*O. occultum* and *O. panamense*) to 9.9% (*O. hendleri* and *O. panamense*) in *Ophioderma* and up to 20.9% (*O. panamense* and *O. fallax*) including *Ophiopeza*. Particularly within the *O. teres*-like group (*O. teres*, *Ophioderma* sp. A, and *Ophioderma* sp. B), COI genetic distances ranged from 3.3% (*O. teres* and *Ophioderma* sp. A) to 8.6% (*O. teres* and *Ophioderma* sp. B), and 16S showed a distance value of 6.1% (*Ophioderma* sp. A and *Ophioderma* sp. B) (Table 3).

The bPTP analyses identified 12 probable species for COI and six for 16S. In both cases, the clades grouping the sequences of *O. teres*, *Ophioderma* sp. A, and *Ophioderma* sp. B were supported as distinct species with high posterior probability values (COI: 0.94–0.99; 16S: 0.71–0.95) (see [Supp. file 7](#)).

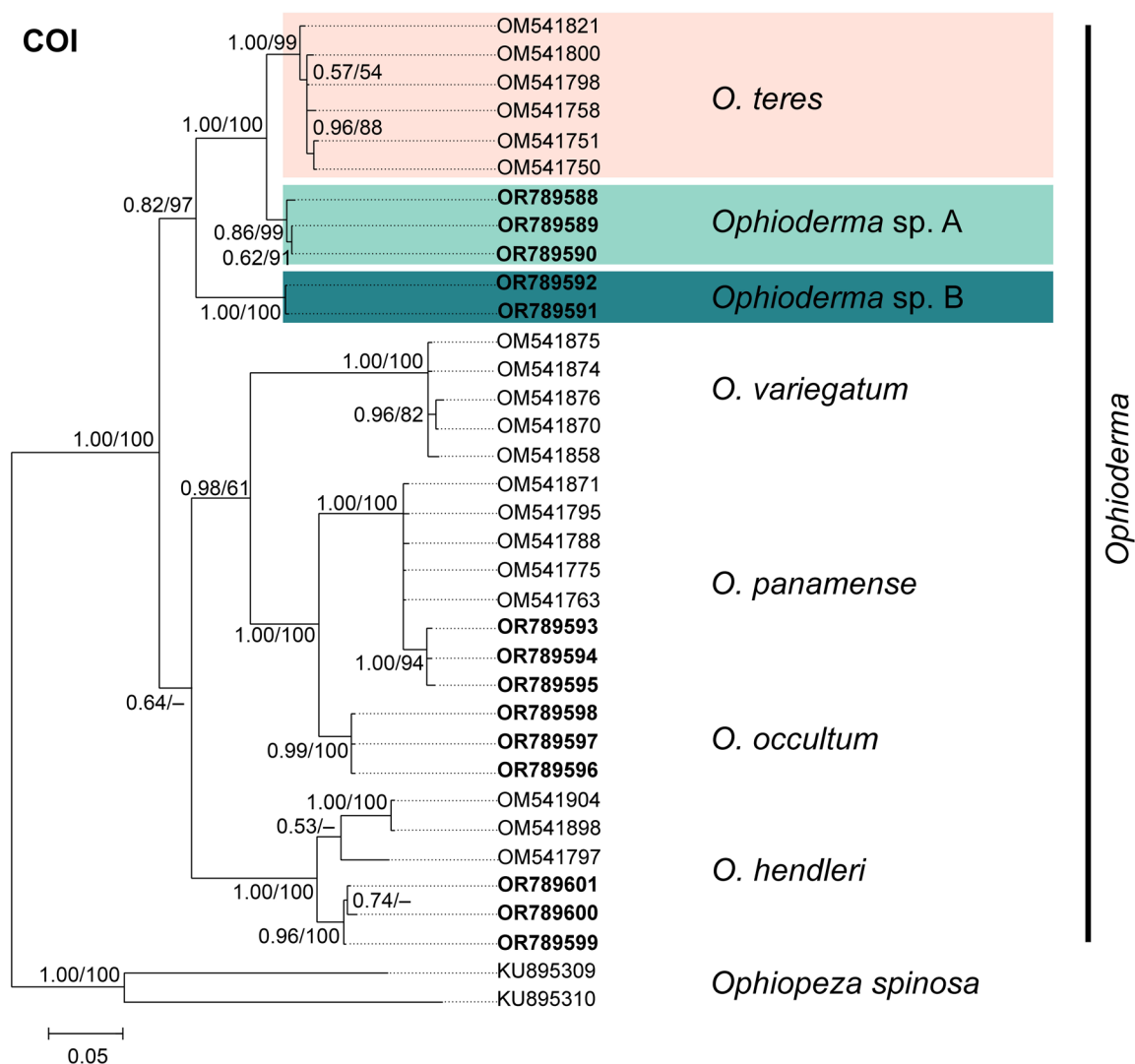


Fig. 1. Bayesian inference (BI) tree of COI sequences. Numbers on branches indicate posterior probability/bootstraps values obtained with BI and maximum likelihood (ML), respectively. A dash (–) indicates the branches not recovered in the ML analysis. Sequences obtained in this study are indicated in bold (see [Supp. file 5](#)).

Table 3. Mean genetic distances (%) between the analyzed species/morphotypes of *Ophioderma* Müller & Troschel, 1840 and *Ophiopeza* Peters, 1851 (COI, lower left; 16S, upper right). A dash (–) indicates no data are available due to a lack of sequences.

Species/morphotype	1	2	3	4	5	6	7	8	9
1 <i>O. hendleri</i>	*	9.6	9.9	–	–	9.7	9.7	19.1	–
2 <i>O. occultum</i>	11.8	*	3.0	–	–	7.4	8.6	19.0	–
3 <i>O. panamense</i>	13.2	6.3	*	–	–	7.4	8.4	20.9	–
4 <i>O. teres</i>	12.3	11.4	12.7	*	–	–	–	–	–
5 <i>O. variegatum</i>	14.0	11.4	12.7	13.0	*	–	–	–	–
6 <i>Ophioderma</i> sp. A	11.7	11.4	12.9	3.3	12.2	*	6.1	18.8	–
7 <i>Ophioderma</i> sp. B	12.5	11.2	12.0	8.6	12.8	8.3	*	18.6	–
8 <i>Ophiopeza fallax</i> ¹	–	–	–	–	–	–	–	*	–
9 <i>Ophiopeza spinosa</i> ²	20.6	19.9	21.7	20.7	21.4	20.5	20.5	NA	*

¹ Outgroup for 16S analyses.

² Outgroup for COI analyses.

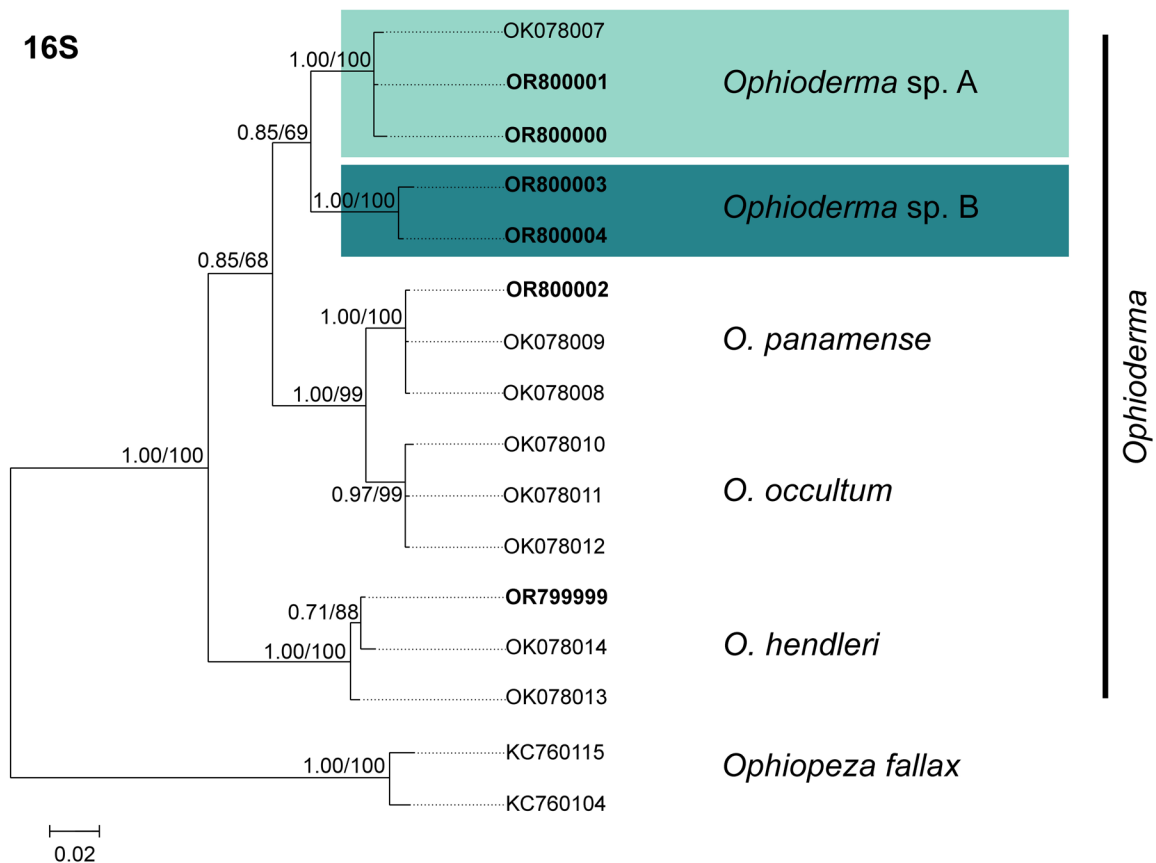


Fig. 2. Bayesian inference (BI) tree of 16S sequences. Numbers on branches indicate posterior probability/ bootstrap values obtained with BI and maximum likelihood, respectively. Sequences obtained in this study are indicated in bold (see [Supp. file 5](#)).

Table 4. Summary of the comparisons of the analyzed evidence by pairs of species/morphotypes of *Ophioderma* Müller & Troschel, 1840. A dash (–) indicates no data are available for one or both species/morphotypes compared.

Type of evidence	Pairs of species/morphotypes				
	<i>O. sodipallaresi</i> / <i>O. teres</i>	<i>O. sodipallaresi</i> / <i>O. teres unicolor</i>	<i>O. sodipallaresi</i> / <i>Ophioderma</i> sp. A	<i>O. sodipallaresi</i> / <i>Ophioderma</i> sp. B	<i>O. teres</i> / <i>O. teres unicolor</i>
External morphology	no differences ¹	differences	differences	differences	differences
Internal morphology	–	–	–	–	–
Morphometrics	no differences	no differences	differences	no differences	differences
COI	–	–	–	–	–
16S	–	–	–	–	–

Type of evidence	Pairs of species/morphotypes				
	<i>O. teres</i> / <i>Ophioderma</i> sp. A	<i>O. teres</i> / <i>Ophioderma</i> sp. B	<i>O. teres unicolor</i> / <i>Ophioderma</i> sp. A	<i>O. teres unicolor</i> / <i>Ophioderma</i> sp. B	<i>Ophioderma</i> sp. A / <i>Ophioderma</i> sp. B
External morphology	differences	differences	differences	differences	differences
Internal morphology	differences	no differences	–	–	differences
Morphometrics	no differences	differences	differences	differences	differences
COI	differences	differences	–	–	differences
16S	–	–	–	–	differences

¹ Considering specimens of similar sizes.

Integrative taxonomy

The analysis of the external and internal morphology, morphometrics, and COI and 16S molecular evidence indicates that *O. teres*, *O. teres unicolor*, *Ophioderma* sp. A, and *Ophioderma* sp. B are distinct species. These showed consistent differences from one another in at least two (e.g., external morphology and morphometrics between *O. teres* and *O. teres unicolor*) and up to five (e.g., external morphology, internal morphology, morphometrics, COI, and 16S between *Ophioderma* sp. A and *Ophioderma* sp. B) of the analyzed types of evidence. The only two exceptions to the latter were *O. teres unicolor* and *Ophioderma* sp. B when compared to *O. sodipallaresi*. In these cases, the data available were the external morphology and morphometrics, with only the former supporting differences between taxa (Table 4). However, the morphological disparities observed in characters typically diagnostic for *Ophioderma* species (Table 1), examined in specimens of different sizes, were considered important enough to treat *O. teres unicolor* and *Ophioderma* sp. B as distinct from *O. sodipallaresi*. Regarding *O. sodipallaresi*, the similarities found between its morphological and morphometric data and those of *O. teres* indicate that they belong to the same species (Table 4). The morphological differences between both taxa were not considered taxonomically relevant, but rather influenced by the size of the specimens examined (see *O. teres* Remarks).

The taxonomic treatment of each recognized species is presented below. This includes 1) the neotype designation and redescription of *O. teres*; 2) the synonymization of *O. sodipallaresi* with *O. teres*; 3) the change of rank from subspecies to species and redescription of *O. teres unicolor*; and 4) the descriptions of *Ophioderma* sp. A (*Ophioderma aija* sp. nov.) and *Ophioderma* sp. B (*Ophioderma bichi* sp. nov.) as new species. In addition, an identification key of the EP *Ophioderma*, including the two new species, is provided.

Systematic account

Phylum Echinodermata Klein, 1778
 Class Ophiuroidea Gray, 1840
 Order Ophiacanthida O’Hara, Hugall, Stöhr & Martynov, 2017
 Suborder Ophiodermatina Ljungman, 1867
 Family Ophiodermatidae Ljungman, 1867
 Genus *Ophioderma* Müller & Troschel, 1840

Ophioderma teres (Lyman, 1860)

Figs 1, 3–6, 12A; Tables 1–4

Ophiura teres Lyman, 1860: 198–200, 257–258 (partim).

Ophioderma sodipallaresi Caso, 1986: 223–248, figs 1–13, **syn. nov.**

Ophiura teres – Lyman 1865: 37–38, fig. 1 (partim).

Ophioderma teres – Ljungman 1867: 304 (comb. nov.). — Nielsen 1932: 332–334, fig. 37. — H.L. Clark 1940: 342. — Zieshenne 1955: 189–190 (partim). — Granja-Fernández 2019: 273–275, fig. 37a–f (partim). — Humara-Gil *et al.* 2022: 373, fig. 4j, table 1.

Ophioderma sodipallaresi – Alvarado *et al.* 2017: 278. — Granja-Fernández 2019: 270–273, fig. 36g–l. — Humara-Gil *et al.* 2022: 373, fig. 4g–i, table 1.

Diagnosis

DAPs divided into multiple pieces (mean = 3, maximum = 13). Coloration light brown to brown; disc and dorsal arms with conspicuous rounded cream specks; ventral arms cream proximally, darkening distally (preserved specimens).

Material examined

Neotype (here designated)

PANAMA • dry preserved specimen; Pearl Islands; 1875; MCZ IZ OPH-113.

Holotype of *Ophioderma sodipallaresi*

MEXICO • dry preserved specimen; Sinaloa, Mazatlán, northwest of Pájaros Island; 23°15'39" N, 106°28'37" W; 9 m depth; 24 Jan. 1983; M.E. Caso, J. Torres Vega, O. López, J. Álvarez, F. Flores, Quijano and Osuna leg.; sandy-rocky substrate; ICML-UNAM 3.24.3.

Paratypes of *Ophioderma sodipallaresi*

MEXICO – Sinaloa • 1 spec. (preserved dry); Mazatlán, in front of Lobos Island; 23°10'32" N, 106°27'55" W; 12 m depth; 4 Sep. 1979; M.E. Caso, J. Torres Vega, F. Flores, J.A. Gamboa, J. Álvarez, G. Díaz and Orozco leg.; rocky-sandy substrate; ICML-UNAM 3.24.0 • 2 specs (preserved dry); Mazatlán, inlet between Lobos Island and Venados Island; 23°13'44" N, 106°27'56" W; 10 m depth; 6 Sep. 1979; M.E. Caso, J. Torres Vega, F. Flores, J.A. Gamboa, J. Álvarez, G. Díaz and Orozco leg.; sandy-rocky substrate; ICML-UNAM 3.24.1 • 1 spec. (preserved dry); Mazatlán, north of Pájaros Island; 23°15'40" N, 106°28'39" W; 4–5 m depth; 18 Mar. 1982; M.E. Caso, J. Torres Vega, O. López, F. González and F. leg.; rocky-sandy substrate; ICML-UNAM 3.24.2 • 1 spec. (preserved dry); Mazatlán, northwest of Pájaros Island; 23°15'39" N, 106°28'37" W; 9 m depth; 24 Jan. 1983; M.E. Caso, J. Torres Vega, O. López, J. Álvarez, F. Flores, Quijano and Osuna leg.; sandy-rocky substrate; ICML-UNAM 3.24.4.

Other material

See [Supp. file 1](#).

Designation of neotype

As one of the most emblematic *Ophioderma* from the EP (Solís-Marín *et al.* 2013), the identity of *O. teres* was considered clear for years. However, recent attempts to study the species revealed that: 1) its type material was missing, and 2) it had been mistaken for similar undescribed species in different scientific collections (Humara-Gil *et al.* 2022; RGF, KJHG pers. obs.). In view of these problems, the designation of a neotype for *O. teres* became necessary to redefine it and clarify its taxonomic status (ICZN 1999, Arts 75.1, 75.3.1).

The holotype of *O. teres* was searched for in the USNM, where it was originally deposited (Lyman 1860), but could not be found. The search for the material in other collections worldwide (i.e., American Museum of Natural History, New York, USA; LACM; MCZ; Museum national d'Histoire naturelle, Paris, France; Natural History Museum of Denmark, University of Copenhagen, Copenhagen, Denmark; UMML; Yale Peabody Museum of Natural History, New Haven, USA) was also unsuccessful. Hence, it was presumed lost or destroyed (ICZN 1999, Art. 75.3.4). The work of Downey (1969) implies that the holotype of *O. teres* might have been lost long ago, as it was not listed in her catalog of Ophiuroidea types despite having included all the USNM material. This indicates that the whereabouts of this material have been unknown since at least 1969.

A neotype for *O. teres* is proposed herein and is comprehensively described and illustrated in accordance with the International Code of Zoological Nomenclature (ICZN) (ICZN 1999, Arts 75.3.2–75.3.3). The selected specimen accords with the original description of the species by Lyman (1860), as well as with other specimens identified by him as *O. teres* (MCZ IZ OPH-112, MCZ IZ OPH-115, MCZ IZ OPH-230) (ICZN 1999, Art. 75.3.5). The neotype was collected in Panama like the original holotype (Lyman 1860; ICZN 1999, Art. 75.3.6), specifically in the Pearl Islands. The latter becomes the new type locality for the species (ICZN 1999, Art. 76.3). The neotype is deposited in the MCZ (ICZN 1999, Art. 75.3.7).

Description

Neotype

DD = 26.5 mm, AL = 110.1 mm, AL:DD = 4.1. Disc pentagonal, covered by minute rounded granules, slightly separated from each other. Granule size varies randomly along disc. Granules rubbed off in some areas, exposing scales underneath. Dorsal disc granule density 70 per mm². Radial shields covered by granules (Fig. 3A). Small, rounded to oval plates of variable size (2–4) close to arm base (Fig. 3A, D). Ventral interradii covered with granules increasing in size the closer they are to disc distal section. Four genital slits per interradius. Proximal genital slits oval, slightly separated from distal section of oral shields by two rows of granules, but in contact with 1st LAP; reaching up to proximal section of 2nd VAP. Distal genital slits oval, longer than proximal ones, placed between 4th and 6th arm segments; surrounded by granule-bearing scales and a few naked scales next to the arm (Fig. 3B).

Oral shields 1.6 × as wide as long, rounded triangular; proximal edge convex forming a rounded apex; lateral edges rounded; distal edge straight. Madreporite oval, with a central depression slightly deviated towards distal section; distal edge convex. Adoral shields covered by small granules, closely grouped. Jaws with 9–11 oral papillae: LyOs 2 × as long as wide, angled upwards; AdShSp the largest, triangular with rounded edges; 2°AdShSp similar in shape to AdShSp, but smaller; LOPas 4–6, rectangular to conical, pointed; IPa similar to LOPas; TPa two at jaw apex, elongated, robust. Teeth five: vT triangular with rounded edges, slightly flattened; median teeth quadrangular; dorsalmost triangular and pointed. One OPRSp at each side of the jaw, conspicuous. Oral plates covered with granules larger than those close to the margin of oral shields (Fig. 3C).

Five arms rounded, tapering distally: all without distalmost segments (Fig. 3K). Dorsal arm base with some small scales and few granules scattered between them (Fig. 3D). DAPs wider than long, typically divided into four and up to seven irregular pieces (Fig. 3D–E). DAP pieces sequence of the longest arm: first ten segments, 5, 5, 4, 4, 4, 4, 4, 5, 4, 5; 11th–20th, 4–6; 21st–30th, 3–5; 31st–40th, 3–5; 41st–50th, 2–5; 51st–60th, 2–3; 61st–70th, 1–4; 71st–80th, 1–2; 81st–89th, 1. Distalmost DAPs trapezoidal to triangular, entire (Fig. 3F). First VAP small, 1.8 × as wide as long, with rounded edges (Fig. 3B). Subsequent VAPs quadrangular, longer than wide proximally to wider than long in the median arm section (Fig. 3G–H); distal edge convex in proximal VAPs (Fig. 3G), slightly concave in median VAPs (Fig. 3H), and convex in distal VAPs (Fig. 3I). Distalmost VAPs triangular with rounded edges, slightly longer than wide (Fig. 3I). A pair of pores between the 2–3 proximalmost VAPs in all five arms (Fig. 3B). LAPs conspicuous, wider than long, with up to 11 arm spines. Arm spine sequence of the longest arm (right side, including arm spine bearing segments within disc): first ten segments, 3, 3, 4, 4, 5, 6, 6, 8, 9, 9; 11th–20th, 9–10; 21st–30th, 9–10; 31st–40th, 8–9; 41st–50th, 7–10; 51st–60th, 8; 61st–70th, 7–8; 71st–80th, 6–7; 81st–90th, 5–6; 81st–90th, 4–5. Arm spines conical with blunt tips, flattened, $\frac{2}{3}$ LAP length. Dorsalmost arm spine the shortest; ventralmost the longest and more robust, covering approximately $\frac{1}{3}$ of the following segment adradial tentacle scale (Fig. 3J). Two tentacle scales, rarely three; adradial tentacle scale oval, elongated, just over $\frac{1}{2}$ VAP length; abradial tentacle scale shorter and wider, $\frac{3}{4}$ adradial scale length, triangular (Fig. 3G–H). In the distalmost arm section, tentacle scales oval and elongated, adradial being the longest; last arm segments with only one scale (Fig. 3I).

General coloration light brown with lighter cream specks (dry specimen) (Fig. 3K). Dorsal side: disc light brown, with subtle clusters of lighter granules (Fig. 3A). Arms light brown with rounded cream specks not following a definite pattern (Fig. 3D–E, K). Ventral side: interradii light brown with clusters of cream granules, giving a non-uniform speckled appearance (Fig. 3B). Oral shields light brown; oral papillae, teeth, and arms cream (Fig. 3B–C). LAPs light brown, some with light specks as those on DAPs. Arm spines beige to light brown; the ventralmost the lighter (Fig. 3J).

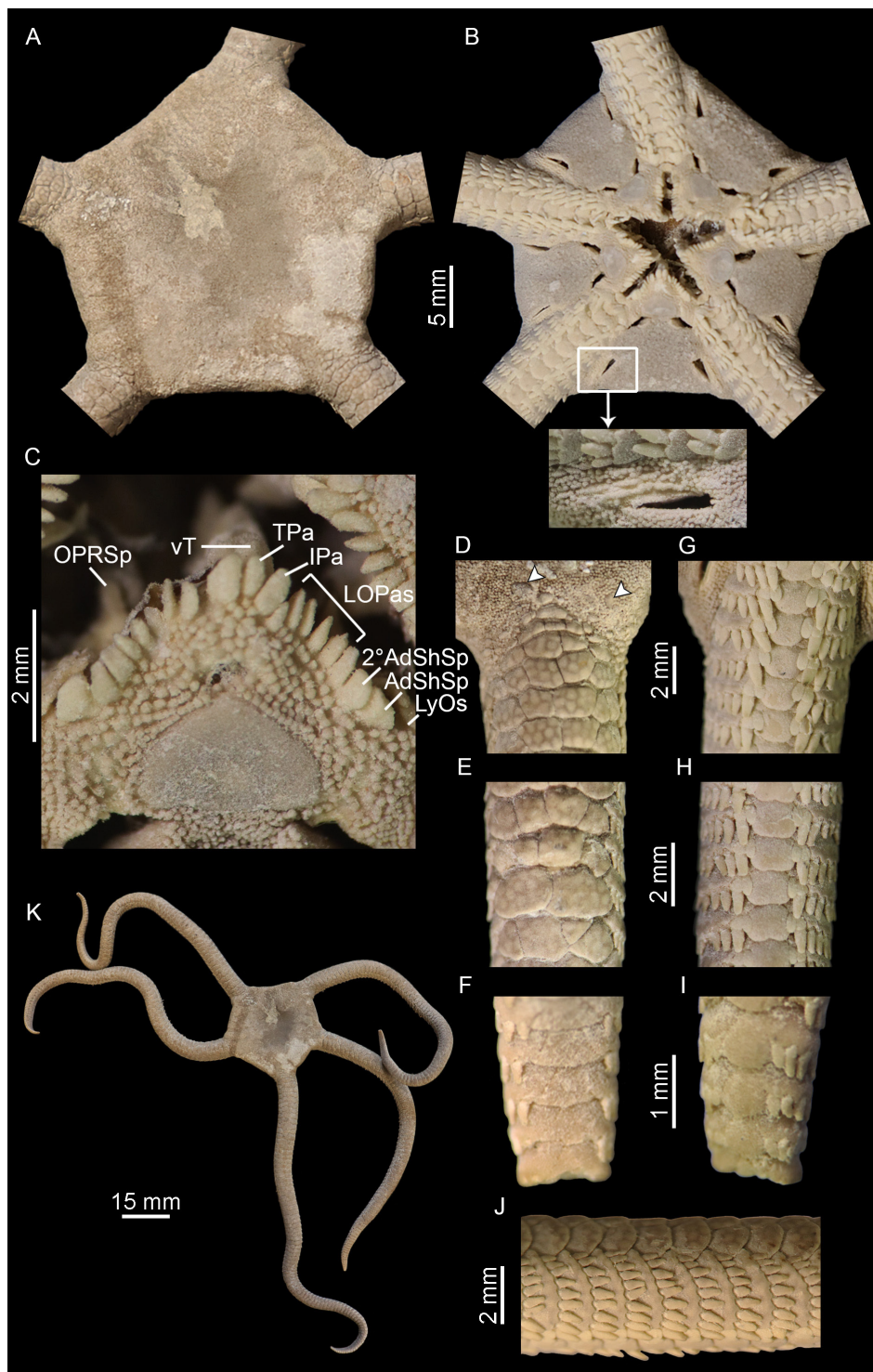


Fig. 3. *Ophioderma teres* (Lyman, 1860), neotype (MCZ IZ OPH-113, DD = 26.5 mm). **A.** Dorsal disc. **B.** Ventral disc (inset: section between the arm and the distal genital slit). **C.** Close-up of a jaw. **D.** Proximalmost dorsal arm. Arrowheads indicate the extra plates on the arm base. **E.** Median dorsal arm. **F.** Distalmost dorsal arm. **G.** Proximalmost ventral arm. **H.** Median ventral arm. **I.** Distalmost ventral arm. **J.** Lateral arm plates and arm spines. **K.** Dorsal view. Abbreviations: 2° AdShSp = secondary adoral shield spine; AdShSp = adoral shield spine; IPa = infradental papilla; LOPas = lateral oral papillae; LyOs = Lyman's ossicle; OPRSp = oral plate ridge spine; TPa = tooth papilla; vT = ventralmost tooth.

Disarticulated ossicles

Non-type specimen, USNM E23201 (DD = 26.9 mm, AL = 83.2 mm, AL:DD = 3.1). Radial shields irregularly triangular, covered in the intact animal; proximal edge convex; distal edge convex; adradial edge irregular with a median process; abradial edge with two processes, distal prominent (Fig. 4A–B). Externally, distal half swollen, with scattered small pores in the center; proximalmost and lateral edges with larger pores (Fig. 4A). Internally, distal half center with three median pores; close to distal edge, two rounded bulbs slightly separated, adradial one larger, followed by a furrow (Fig. 4B). Dental plate fragmented into several pieces (up to six), each supporting one or two teeth in oval or round non-penetrating sockets (Fig. 4C). Adradial genital plate falcate, elongated, widening distally, with a longitudinal groove and a large pore close to distal section. Distal edge rounded, with a lateral protuberance (Fig. 4D). Oral plates longer than high, fragmented during disarticulation (Fig. 4E–F); abradial muscle fossa irregularly triangular, widening ventrally (Fig. 4E). Vertebrae zygospondylus (Fig. 4G–H). Proximal vertebrae wider than long, with dorsal muscle fossae larger than ventral ones (Fig. 4G). VAPs (from proximal arm section) quadrangular, slightly longer than wide; proximal edge with three points, the median and larger one corresponding to a spur; lateral edges with two points forming concave areas; distal edge concave (Fig. 4I). Internal face with three spurs, two elongated and lateral, and one middle smaller and rounded (Fig. 4J). LAPs curved, 2 × as high as wide; dorsal edge straight; ventral edge slightly convex, with a small, rounded condyle developing from internal side; proximal edge concave; distal edge convex (Fig. 4K–M). Proximal external edge with two elongated, conspicuous spurs in the middle (Fig. 4K), having their counterparts internally (Fig. 4L). Internal side with four pores near center, concave proximal ridge, and two separated bulbs near ventral edge, the ventralmost protruding from plate. Ten spine articulations on distal edge, each surrounded by a thick lobe (Fig. 4M).

Non-type variations

Non-type specimens varied in size from 11.6 to 33.8 mm (DD). Fourteen specimens (DD = 11.8–33.8 mm), including two larger than the neotype (DD = 26.7 and 33.8 mm), showed naked radial shields, oval (rarely rounded) and 1.5 × as long as wide. One specimen (DD = 19.2 mm) had nine partially visible radial shields. One of the largest specimen (DD = 32.9 mm) presented noticeable covered radial shields sunken into the disc. All the examined specimens with DD < 20 mm lacked plates on their discs, while 12 larger ones (DD = 20.1–32.9 mm) had between one and four small, rounded plates near the arm base, like the neotype. Three specimens (DD = 11.6, 13.7, and 17.4 mm) only had granule-bearing scales in the section between the arm and the distal genital slit, instead of naked and granule-bearing scales like the remaining specimens. Nine specimens showed trilobed rather than rounded triangular oral shields. Eight specimens (DD = 16.5–33.5 mm) exhibited a few granules between the edges of 2–7 proximalmost DAPs. All specimens presented DAPs divided into multiple pieces; the smaller the specimen, the less fragmented the DAPs were. The smallest specimen (DD = 11.6 mm) had the highest number of entire DAPs, with only a few divided into two pieces; in the largest (DD = 33.8 mm), the mean number of DAP pieces increased to five pieces with a maximum of nine. The maximum number of arm spines also varied with size, ranging from seven (DD = 11.8 and 13.0 mm) to 12 (DD = 29.1, 32.6, and 33.5 mm). Two specimens (DD = 17.5 and 32.9 mm) presented a few segments with three tentacle scales; the remaining specimens showed two tentacle scales on each segment.

The remaining variations were observed in coloration. Five specimens displayed a brown center on their dorsal disc, with the cream specks limited to the disc periphery. One specimen had some groups of brown granules resembling brown specks, in addition to the usual cream-colored ones. In three specimens, the radial shields were completely brown, and in another they had a single central cream-colored speck. Eighteen specimens showed brown oral shields with cream specks (comparable to those observed on DAPs and radial shields); another presented cream-colored oral shields with a brown center. In four specimens, the ventral arms darkened distally. These differences likely resulted from preservation.

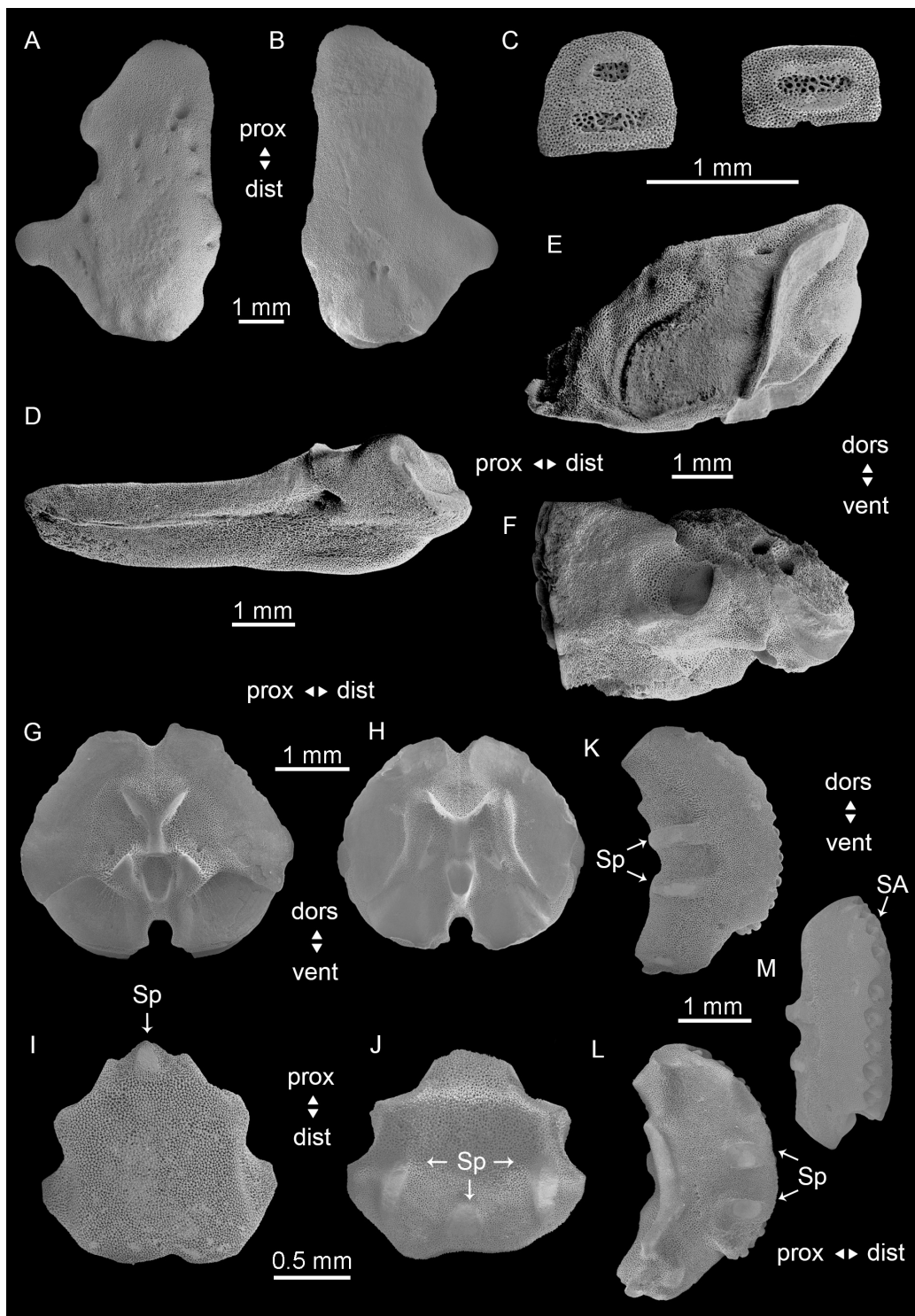


Fig. 4. *Ophioderma teres* (Lyman, 1860), non-type specimen (USNM E23201, DD = 26.9 mm), SEM images of the ossicles. **A.** Radial shield, external face. **B.** Radial shield, internal face. **C.** Dental plate. **D.** Adradial genital plate, adradial face. **E.** Oral plate, abradial face. **F.** Oral plate, adradial face. **G.** Arm vertebra, proximal face. **H.** Arm vertebra, distal face. **I.** Ventral arm plate, external face. **J.** Ventral arm plate, internal face. **K.** Lateral arm plate, external face. **L.** Lateral arm plate, internal face. **M.** Lateral arm plate, lateral face. Abbreviations: dist = distal; dors = dorsal; prox = proximal; SA = spine articulation; Sp = spur; vent = ventral.

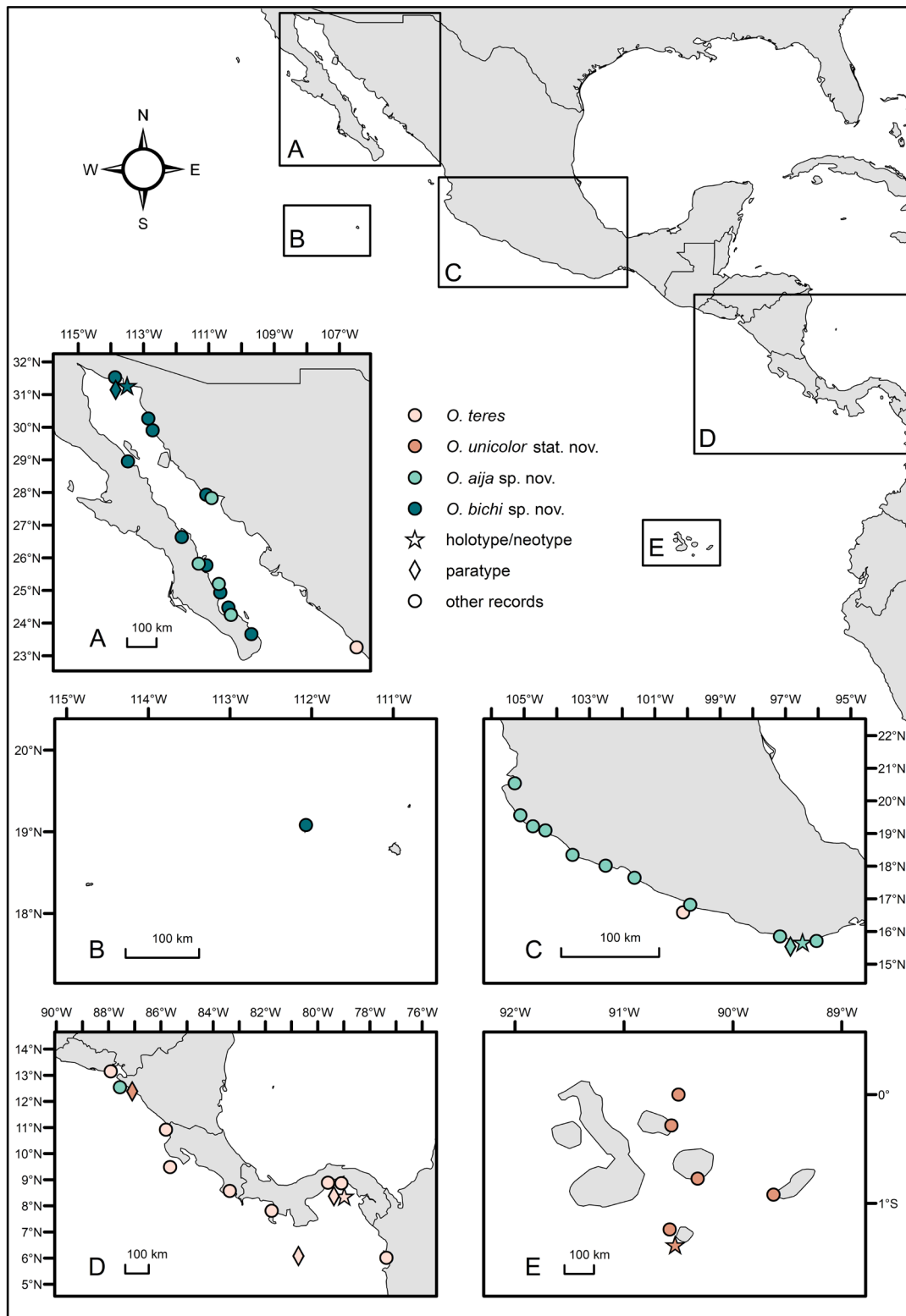


Fig. 5. Distribution of *Ophioderma teres* (Lyman, 1860), *Ophioderma unicolor* H.L. Clark, 1940 stat. nov., *Ophioderma aija* sp. nov., and *Ophioderma bichi* sp. nov. in the eastern Pacific. **A.** Gulf of California. **B.** Revillagigedo Islands. **C.** Mexican Tropical Pacific. **D.** Central America and Colombia. **E.** Galapagos Islands.

Distribution and habitat

Ophioderma teres was presumed to be widely distributed in the EP, from the southwestern USA to Peru (Maluf 1988; Granja-Fernández & Hooker 2020), but its distribution appears more restricted. In Mexico, the species was collected in Sinaloa and Guerrero; in El Salvador, in Maculís; in Costa Rica, in Port Parker (now Bahía de Santa Elena), Parque Nacional Marino Ballena, and Golfo Dulce; in Panama, in the Gulf of Chiriquí, Gulf of Panama, and the Pearl Islands, and in Colombia, in Port Utria (see [Supp. file 1](#)). Its northernmost record corresponds to Pájaros Island, Sinaloa, Mexico (23° N; as *O. sodipallaresi*, see Remarks), and the southernmost to Port Utria, Colombia (5° N) (Fig. 5).

Records of *O. teres* in previous studies should be carefully evaluated using voucher material to verify or refute its presence at the reported locations. For example, in Mexico the species had been reported in Baja California, Baja California Sur, Nayarit, Jalisco, and Oaxaca (Honey-Escandón *et al.* 2008; Granja-Fernández *et al.* 2015). However, these records are now considered invalid as they pertain to *O. occultum* or the two newly described species below (*O. aija* sp. nov., *O. bichi* sp. nov.). Although the species has also been reported in the USA, Nicaragua, Ecuador, and Peru (Solís-Marín *et al.* 2013), no material from these countries belonging to *O. teres* was found in the collections visited. Based on the data available from the revised specimens, *O. teres* inhabits tide pools, sandy mud, sandy spits, and rocks, and can be found at depths of up to 10 m.

Remarks

Once considered quite variable in morphology and widespread in the EP, *O. teres* is now recognized to have been consistently confused with different known and new species (Lyman 1860, 1865; Nielsen 1932; H.L. Clark 1940; Ziesenhene 1955; Granja-Fernández 2019).

One of the species with the most striking resemblance to *O. teres* is *O. sodipallaresi*. Both have covered or naked radial shields (Fig. 6A–B), covered adoral shields (Fig. 6C–D), divided DAPs (Fig. 6G–J), and the characteristic cream-colored specks on their discs and arms (Fig. 6). However, they differ in size (*O. sodipallaresi*: DD up to 20.9 mm; *O. teres*: DD up to 33.8 mm), distal genital slit ornamentation (*O. sodipallaresi*: granule-bearing scales (Fig. 6E); *O. teres*: naked and granule-bearing scales (Fig. 6F)), number of pieces of their divided DAPs (*O. sodipallaresi*: mean = 2, maximum = 5; *O. teres*: mean = 3, maximum = 13), and maximum number of arm spines (*O. sodipallaresi*: 10; *O. teres*: 12). The last three characters are known to vary in *Ophioderma* according to the size, though (Granja-Fernández *et al.* 2020; Stöhr *et al.* 2020; Humara-Gil *et al.* 2022). Specimens of *O. teres* close in size (DD = 11.6–21.6 mm) (Fig. 6B, D, F, I–J) to the type series of *O. sodipallaresi* (DD = 9.9–20.9 mm) (Fig. 6A, C, E, G–H) had similar counts of DAPs pieces and arm spines, with the smallest one having only granules on its distal genital slit. Considering the above, *O. sodipallaresi* is herein regarded as a junior synonym of *O. teres*. Caso (1986) may have overlooked the similarities between her then new species, *O. sodipallaresi*, and *O. teres* because she had been identifying other species (*O. aija* sp. nov., *O. bichi* sp. nov.) as the latter (Caso 1951; RGF, KJHG pers. obs.) and had not examined specimens of *O. teres* *sensu stricto* before.

It is worth noting that the specimens described by Caso (1986) from Sinaloa as *O. sodipallaresi*, and two specimens from Acapulco (MCZ IZ OPH-112), were the only material of *O. teres* from Mexico in the collections visited. Despite the ongoing collection of ophiuroids along the Mexican Pacific coast for the past ~13 years (RGF pers. obs.), the species has not been found again in the region. This contrasts with what has been observed in other countries, such as Costa Rica, where the species appears to be conspicuous and abundant (Chacón-Monge 2019 pers. com.).

Ophioderma teres most resembles *O. peruanum*, with which it shares the covered or naked radial shields, covered adoral shields, distal genital slit ornamentation, divided DAPs, and color pattern. On the other

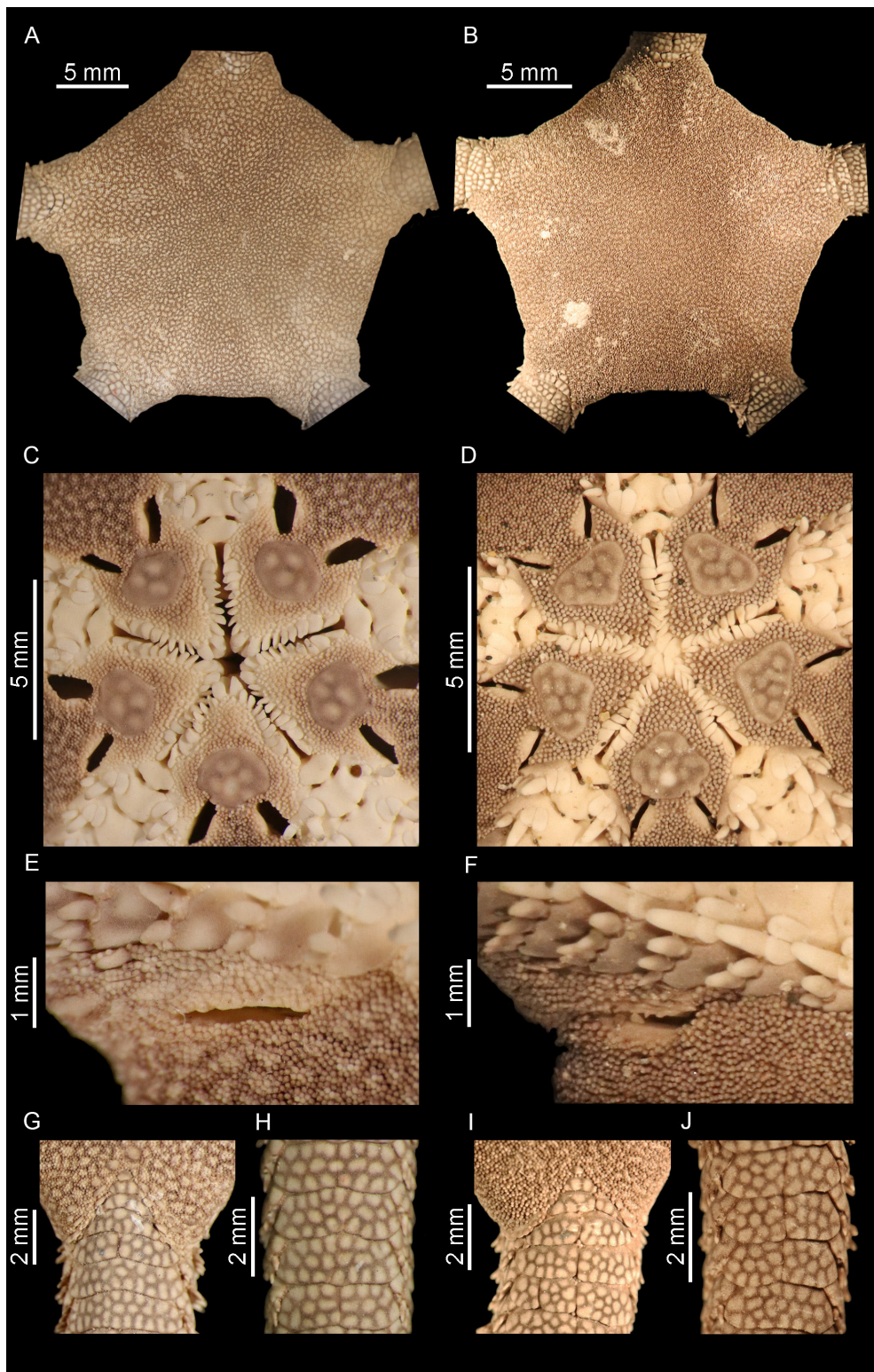


Fig. 6. Comparison between *Ophioderma sodipallaresi* Caso, 1986 (= *Ophioderma teres* (Lyman, 1860)), holotype from Mexico (ICML-UNAM 3.24.3, DD = 20.9 mm) (left), and *Ophioderma teres*, non-type material from Panama (USNM E23215, DD = 19.3 mm) (right). **A–B.** Dorsal disc. **C–D.** Jaws. **E–F.** Section between the arm and the distal genital slit. **G, I.** Dorsal arm (proximalmost). **H, J.** Dorsal arm (median).

hand, they differ in the size and density of the disc granules (*O. teres*: scattered, of different sizes along the disc; *O. peruanum*: closely packed, of uniform size), extent of granules on the arms (*O. teres*: limited to the arm base; *O. peruanum*: on the distal part of the proximalmost and median DAPs), and geographic distribution (*O. teres*: from Mexico to Panama; *O. peruanum*: only known from Peru) (Pineda-Enríquez *et al.* 2013). Despite the previous findings, the taxonomic status of *O. peruanum* remains unclear due to the limited number of specimens examined ($n = 4$). It is uncertain whether this species is distinct from *O. teres* or represents its southernmost record instead. Additional research incorporating morphological and molecular data is needed to elucidate the taxonomic status of *O. peruanum*.

Ophioderma unicolor H.L. Clark, 1940 stat. nov.
Figs 5, 7; Tables 1–2, 4

Ophioderma teres var. *unicolor* H.L. Clark, 1940: 342.

Ophioderma teres – Ziesenhenné 1955: 191 (partim, non Lyman, 1860). — Hickman 1998: 24 (partim, non Lyman, 1860).

Ophioderma teres var. *unicolor* – Downey 1969: 115 (partim). — Granja-Fernández 2019: 275–279, fig. 37g–l (partim).

Ophioderma teres unicolor – Humara-Gil *et al.* 2022: 373, fig. 4k, table 1 (stat. nov.).

Diagnosis

Radial shields naked. DAPs divided into multiple pieces (mean = 2, maximum = 6). Coloration uniform brown (preserved specimens).

Material examined

Holotype

ECUADOR • dry preserved specimen; Galapagos Islands, Charles Island; 1872; Hassler Expedition leg.; MCZ IZ OPH-114.

Paratype

NICARAGUA • 1 spec. (preserved dry); Corinto, Cardon Island; 12°28'28" N, 87°10'51" W; 3.6 m (2 fathoms) depth; 29–30 Dec. 1937; Zaca Expedition leg.; MCZ IZ OPH-6153.

Other material

See [Supp. file 1](#).

Designation of the new status as species

Ophioderma teres unicolor was initially considered a variety of *O. teres* (H.L. Clark, 1940) and later categorized as a subspecies based on the ICZN (ICZN 1999, Art. 45.6.4) (Humara-Gil *et al.* 2022). However, the detailed examination of both taxa revealed differences in characters that are diagnostic at the species level within the genus. *Ophioderma teres unicolor* has naked radial shields, DAPs divided into up to six pieces, and a uniform brown coloration. On the other hand, *O. teres* presents radial shields that may be covered or naked, DAPs divided into up to 13 pieces, and a speckled color pattern. Given the differences in these relevant characters, a new status for *O. teres unicolor* is herein proposed, raising its rank from subspecies to species: *O. unicolor* stat. nov.

Description

Holotype

DD = 35.7 mm, AL = 128 mm, AL:DD = 3.6. Disc pentagonal, covered by minute rounded granules, slightly separated from each other. Granule size increasing from center to periphery and decreasing

close to arm base. Some granules rubbed off, leaving scales visible. Dorsal disc granule density 39 per mm². Radial shields naked; visible section approximately 1.5 × as long as wide, oval; distance between radial shields about 3 × width of shield (Fig. 7A). Small, oval plates of variable size (up to six) close to arm base (Fig. 7A, D). Ventral interradii covered with small granules of uniform size, separated from each other. Four genital slits per interradius. Proximal genital slits oval, in contact with distal section of oral shields and 1st LAP. Distal genital slits oval, slightly longer than proximal ones, placed between 7th and 9th arm segments; surrounded by granule-bearing scales and naked scales next to the arm (Fig. 7B).

Oral shields 1.2 × as wide as long, rounded triangular; proximal edge convex forming a rounded apex; lateral edges rounded; distal edge straight to concave. Madreporite rounded, broken in two pieces (a probable artifact of preservation), with a central depression; distal edge slightly concave. Adoral shields covered by small granules slightly separated from each other. Jaws with 9–11 oral papillae: LyOs the largest, 2 × as long as wide, angled upwards; AdShSp rounded triangular, pointed; 2°AdShSp similar in shape but slightly smaller than AdShSp; LOPas 3–6, conical, slender; IPa similar to LOPas, more robust; TPa 2–3 at jaw apex, pointed, robust. Teeth five, robust, rounded triangular to quadrangular. OPRSp not evident due to closed mouth. Oral plates covered with granules larger than those covering the adoral shields (Fig. 7C).

Five arms rounded, tapering distally: two almost complete, one regenerating close to arm base and two regenerating from mid-section (Fig. 7K). Dorsal arm base with some small scales and few granules scattered between them (Fig. 7D). DAPs wider than long, typically divided into three and up to six irregular pieces (Fig. 7D–E). DAP pieces sequence of the longest arm: first ten segments, 2, 2, 2, 1, 1, 2, 3, 4, 3, 1; 11th–20th, 1–5; 21st–30th, 2–4; 31st–40th, 3–5; 41st–50th, 3–6; 51st–60th, 2–4; 61st–70th, 3–5; 71st–80th, 2–4; 81st–90th, 2–4; 91st–100th, 2–4; 101st–110th, 1–3; 111st–117th, 1–3. Distal-most DAPs trapezoidal to triangular, entire (Fig. 7F). First VAP small, 3 × as wide as long, with rounded edges (Fig. 7B). Subsequent VAPs quadrangular, slightly longer than wide; distal edge convex (Fig. 7G–H). Distal-most VAPs triangular, rounded, slightly longer than wide (Fig. 7I). A pair of pores between the 3–4 proximal-most VAPs in all five arms (Fig. 7B). LAPs conspicuous, wider than long, with up to 13 arm spines. Arm spine sequence of the longest arm (right side, including arm spine bearing segments within disc): first ten segments, 3, 3, 4, 4, 5, 6, 7, 8, 9, 10; 11th–20th, 12–13; 21st–30th, 11–12; 31st–40th, 11–12; 41st–50th, 10–11; 51st–60th, 10–11; 61st–70th, 9–10; 71st–80th, 8–9; 81st–90th, 8–10; 91st–100th, 7–8; 101st–110th, 6–8; 111th–120th, 6–8; 121st–126th, 4–5. Arm spines conical with blunt tips, flattened, $\frac{2}{3}$ LAP length. Dorsal-most arm spine the shortest; ventral-most the longest and more robust, in contact with tentacle scales of the following segment (Fig. 7J). Two tentacle scales, rarely three; adradial tentacle scale oval, just over $\frac{1}{2}$ VAP length; abradial tentacle scale shorter and wider, $\frac{3}{4}$ adradial scale length, triangular (Fig. 7G–H). In the distal-most arm section, tentacle scales oval and elongated, adradial being the longest; last arm segments with only one scale (Fig. 7I).

General coloration uniform brown (dry specimen) (Fig. 7K). Dorsal side: disc brown (Fig. 7A). Arms brown (Fig. 7D–F, K). Ventral side: interradii brown (Fig. 7B). Oral shields brown; oral papillae and teeth cream (Fig. 7B–C). LAPs brown. Arm spines brown with cream bases and tips (Fig. 7J).

Paratype and non-type variations

The paratype was 29.7 mm in size (DD). It overall agreed with the holotype but differed in the following aspects: its oral shields were trilobed rather than rounded triangular, the 20 proximal-most DAPs were divided into more pieces (mostly four), and the maximum number of spines was 12 instead of 13.

Non-type specimens varied in size from 17.1 to 30.2 mm (DD). In three specimens (DD = 17.1–20.7 mm), the distance between the radial shields was two times the shield width, smaller than in the holotype. In

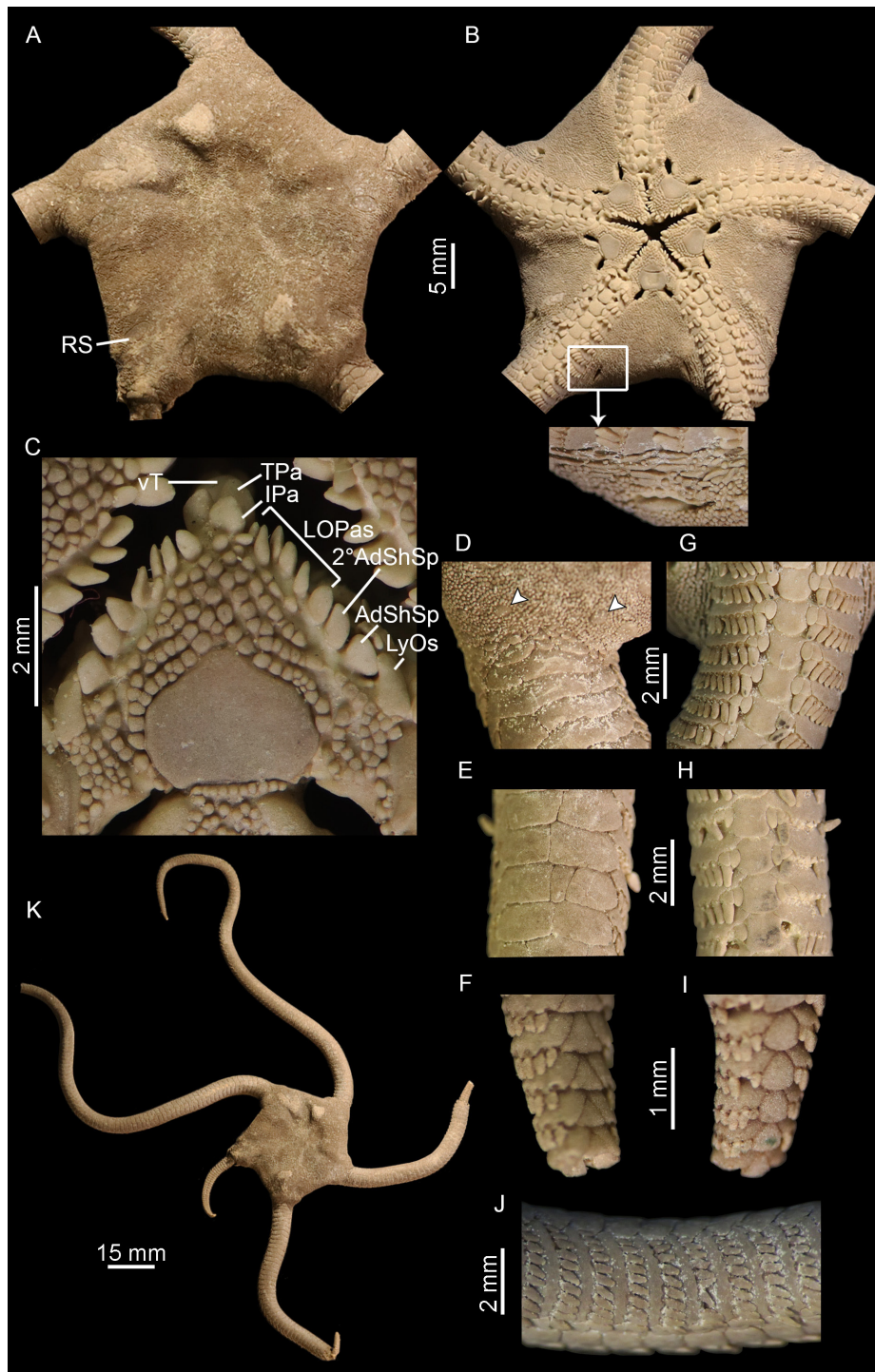


Fig. 7. *Ophioderma unicolor* H.L. Clark, 1940 stat. nov., holotype (MCZ IZ OPH-114, DD = 35.7 mm). **A.** Dorsal disc. **B.** Ventral disc (inset: section between the arm and the distal genital slit). **C.** Close-up of a jaw. **D.** Proximalmost dorsal arm. Arrowheads indicate the extra plates on the arm base. **E.** Median dorsal arm. **F.** Distalmost dorsal arm. **G.** Proximalmost ventral arm. **H.** Median ventral arm. **I.** Distalmost ventral arm. **J.** Lateral arm plates and arm spines. **K.** Dorsal view. Abbreviations: 2° AdShSp = secondary adoral shield spine; AdShSp = adoral shield spine; IPa = infradental papilla; LOPas = lateral oral papillae; LyOs = Lyman's ossicle; RS = radial shield; TPa = tooth papilla; vT = ventralmost tooth.

another specimen (DD = 30.2 mm), the distance was four times the shield width. One specimen (DD = 20.5 mm) presented small plates on the disc near the arm base, while the remainder only had granules. All specimens showed divided DAPs, but two of them (DD = 20.5 and 20.7 mm) had more entire rather than divided plates, with the latter composed of two pieces at most. The maximum number of arm spines varied by size, ranging from ten (DD = 17.1 mm) to 13 (DD = 30.2 mm). Finally, the coloration varied as follows: two specimens, including the one with the lightest general coloration, presented some slightly darker granules on the dorsal disc, particularly in the center; the radial shields were either darker than the disc or the same color but with a significantly darker margin.

Distribution and habitat

Ophioderma unicolor stat. nov. was previously recorded in Mexico, Nicaragua, and Ecuador as *O. teres* var. *unicolor* (H.L. Clark 1940; Downey 1969; Mireles-Velázquez *et al.* 2021). This study confirms its presence in Nicaragua (Cardon Island) and Ecuador (Galapagos Islands) (see [Supp. file 1](#)). On the other hand, the records from Mexico are invalidated as they correspond to a new species described below (*O. aija* sp. nov.). The northernmost record of *O. unicolor* is from Cardon Island, Corinto, Nicaragua (12° N), and the southernmost from Chatham Island (also known as San Cristóbal Island), Galapagos Islands, Ecuador (0° S) (Fig. 5). This species has been collected in rocks, sand, and algae, at depths from 3.6 to 45.7 m.

Remarks

While establishing *O. unicolor* stat. nov., H.L. Clark (1940: 342) designated MCZ IZ OPH-114 as “the type” (= holotype) of the then variety (ICZN 1999, Art. 73.1.1). He also noted that a specimen from Cardon Island, Nicaragua, “very similar” to the holotype, was in the same collection, along with two other specimens (MCZ IZ OPH-6153) (H.L. Clark 1940). H.L. Clark (1940) did not formally acknowledge the latter three specimens as paratypes but neither excluded them from its type series (ICZN 1999, Art. 72.4.6). Downey (1969) treated those specimens as paratypes of *O. unicolor* but reported the lot with two specimens instead of three; the third specimen was likely lost. In accordance with the ICZN, Downey’s (1969) inclusion of these specimens in the type series was appropriate at the time (ICZN 1999, Art. 72.4.1). Nonetheless, the recent examination of the material revealed that one of the specimens (currently MCZ IZ OPH-167471, DD = 10.6 mm) did not correspond to *O. unicolor* but to a different species (see *O. aija* sp. nov. Remarks). Consequently, the type series of *O. unicolor* now comprises the holotype and one paratype.

Ophioderma unicolor stat. nov. has often been misidentified as *O. teres* (Ziesenhenné 1955; Hickman 1998; Granja-Fernández 2019; KJHG pers. obs.), but there are morphological differences between both species (see Designation of the new status as species). Despite the frequent confusion with *O. teres*, *O. bichi* sp. nov. from the EP (described below) and *Ophioderma cinereum* Müller & Troschel, 1842 from the western Atlantic are more similar in appearance to *O. unicolor*. The three species share the covered adoral shields, DAPs divided into multiple pieces, and brown coloration. However, they differ in the following: 1) naked radial shields (sometimes with a darker margin) in *O. unicolor* and *O. cinereum* but covered in *O. bichi*; 2) section between the arm and distal genital slits with naked and granule-bearing scales in *O. unicolor* and *O. cinereum*, and only with granule-bearing scales in *O. bichi*; 3) arms uniformly brown in *O. unicolor* and *O. bichi* but banded in *O. cinereum*; and 4) *O. unicolor* is distributed in the Pacific coast of Central America and the Galapagos Islands, *O. bichi* in the Gulf of California and the Revillagigedo Islands, and *O. cinereum* from the Bahamas to Brazil (Hendler *et al.* 1995; Hernández-Herrejón *et al.* 2008; Gondim *et al.* 2013).

Ophioderma aija sp. nov.

urn:lsid:zoobank.org:act:E2101504-18BC-489E-B65E-CC334EF256D8

Figs 1–2, 5, 8–9, 12B; Tables 1–4

Ophioderma teres – Lyman 1860: 258 (partim, non Lyman, 1860); 1865: 38 (partim, non Lyman, 1860). — Steinbeck & Ricketts 1941: 391–392 (partim, non Lyman, 1860). — Caso 1951: 258–265, figs 21–24 (partim, non Lyman, 1860). — Ziesenhenné 1955: 190–191 (partim, non Lyman, 1860). — Granja-Fernández & López-Pérez 2011: 1321–1322 (non Lyman, 1860). — Granja-Fernández *et al.* 2014: 134–135, fig. 6g–l (non Lyman, 1860).

Ophioderma teres var. *unicolor* – H.L. Clark 1940: 342 (partim, non H.L. Clark, 1940). — Downey 1969: 115 (partim, non H.L. Clark, 1940). — Granja-Fernández 2019: 277–279 (partim, non H.L. Clark, 1940). — Mireles-Velázquez *et al.* 2021: 317–319, fig. 2e–f (non H.L. Clark, 1940).

Ophioderma cf. *teres unicolor* – Humara-Gil *et al.* 2022: 367, 379–380, fig. 5 (partial DNA sequences of genes COI and 16S).

Ophioderma sp. – Granja-Fernández *et al.* 2022: 5, 9.

Ophioderma sp. A – This study: 3–12, Figs 1–2, Tables 1–4.

Diagnosis

Radial shields naked. Arms short (mean AL:DD = 2.7). DAPs divided into multiple pieces (mean = 3, maximum = 9). Coloration dark brown; dorsal and ventral disc with dark, sinuous rings; dorsal arms brown; ventral arms cream (preserved specimens) or yellow (in vivo specimens) proximally, darkening distally.

Etymology

The specific epithet *aija* combines the first two letters of the given names of Aida Janet Gil-Rabadán, mother of the first author. Born under a lucky star, she deserves her own on Earth.

Material examined

Holotype

MEXICO • spec. preserved in 70% ethanol; Oaxaca, La Mina; 15°40.43' N, 96°28.60' W; May 2008; ICML-UNAM 18466.

Paratypes

MEXICO – Oaxaca • 4 specs (preserved in 70% ethanol); Estacahuite; 3.0–12.2 m depth; 3 Mar. 2009; D. Arellanes-García and F. Benítez-Villalobos leg.; sand under dead coral and rocks; ICML-UNAM 18467 • 5 specs (preserved in 96% ethanol); Estacahuite; 15°40'6" N, 96°28'52" W; 9 m depth; 20 Feb. 2020; R. Granja-Fernández leg.; rocks; ICML-UNAM 18468 • 2 specs (preserved dry); Tijera; 15°41'15" N, 96°26'31" W; 10 m depth; 21 Feb. 2020; R. Granja-Fernández leg.; rocks; DNA voucher spec. labelled as “OJ5”; GenBank: OR789590 (COI), OR800000 (16S); ICML-UNAM 18469.

Other material

See [Supp. file 1](#).

Description

Holotype

DD = 26.7 mm, AL = 78.9 mm, AL:DD = 3. Disc rounded, covered by rounded granules, slightly separated from each other. Granule size increasing from center to periphery. Dorsal disc granule density 60 per mm². Radial shields naked; visible section approximately 1.5 × as long as wide, oval; distance between shields about 4 × width of shield (Fig. 8A). Ventral interradii covered with granules of uniform

size, slightly separated from each other. Four genital slits per interradius. Proximal genital slits oval, separated from distal section of oral shields by two rows of granules, but in contact with 1st LAP; reaching up to proximal section of 2nd VAP. Distal genital slits oval, 1.5 × as long as proximal ones, placed between 7th and 9th arm segments; surrounded by granule-bearing scales and naked scales next to the arm (Fig. 8B).

Oral shields 1.6 × as wide as long, rounded triangular; proximal edge convex forming a rounded apex; lateral edges rounded; distal edge straight. Madreporite rounded trapezoidal, with a central depression deviated towards distal section; distal edge convex. Adoral shields covered by small granules. Jaws with 8–9 oral papillae: LyOs 3.5 × as long as wide, angled upwards; AdShSp the largest, trapezoidal; 2°AdShSp smaller than AdShSp, rounded rectangular; LOPas 3–5, rounded rectangular to conical; IPa similar to LOPas, larger; TPa two at jaw apex, triangular to rectangular, robust. Teeth 4–5: vT triangular, slightly flattened; median and dorsalmost teeth quadrangular. One OPRSp on each side of the jaw, conspicuous. Oral plates covered with granules larger than those covering adoral shields, decreasing in size towards periphery (Fig. 8C).

Five arms rounded, tapering distally: all incomplete, three regenerating, the remainder without the distalmost segments (Fig. 8K). Dorsal arm base with multiple scales extending to 1–2 arm segments (Fig. 8D). DAPs wider than long, typically divided into two and up to five irregular pieces (Fig. 8D–E). DAP pieces sequence of the longest arm: first ten segments, 3, 3, 4, 5, 5, 5, 4, 4, 5, 5; 11th–20th, 3–4; 21st–30th, 2–4; 31st–40th, 2–5; 41st–50th, 1–3; 51st–60th, 1–2; 61st–70th, 1–2; 71st–74th, 1. Distalmost DAPs trapezoidal to triangular, entire (Fig. 8F). First VAP small, 2 × as wide as long, with rounded edges (Fig. 8B). Subsequent VAPs quadrangular, longer than wide; proximal edge straight, distal edge convex (Fig. 8G–H). Distalmost VAPs triangular, rounded, wider than long (Fig. 8I). A pair of pores between the two proximalmost VAPs in all five arms (Fig. 8B). LAPs conspicuous, wider than long, with up to ten arm spines. Arm spine sequence of the longest arm (right side, including arm spine bearing segments within the disc): first ten segments, 3, 3, 3, 4, 5, 5, 6, 7, 8, 9; 11th–20th, 9–10; 21st–30th, 9–10; 31st–40th, 8–9; 41st–50th, 8; 51st–60th, 6–8; 61st–70th, 6–7; 71st–80th, 4–6; 81st–83rd, 4. Arm spines conical with blunt tips, slightly flattened, $\frac{2}{3}$ LAP length. Dorsalmost arm spine the shortest; ventralmost the longest and more robust, in contact with tentacle scales of the following segment (Fig. 8J). Two tentacle scales; adradial tentacle scale oval, elongated, just over $\frac{2}{3}$ VAP length; abradial tentacle scale shorter and wider, $\frac{3}{4}$ adradial scale length, triangular (Fig. 8G–H). In the distalmost arm section, tentacle scales oval and elongated, adradial being the longest; last arm segments with only one scale (Fig. 8I).

General coloration dark brown (specimen in ethanol) (Fig. 8K). Dorsal side: disc dark brown with darker, sinuous rings; these may or may not continue over radial shields. Radial shields lighter brown (Fig. 8A). Arms brown, lighter than disc (Fig. 8D–F, K). Ventral side: interradii lighter than dorsal disc, with dark, sinuous rings (Fig. 8B). Oral shields light brown, two with small, darker specks; oral papillae, teeth, and arms cream (Fig. 8B–C). Ventral arms darkening towards the distalmost arm section. LAPs light brown. Arm spines light brown; the ventralmost the lighter (Fig. 8J).

Disarticulated ossicles

Non-type specimen, ICML-UNAM 18457 (DD = 26.2 mm, AL = 81.9 mm, AL:DD = 3.1). Radial shields irregularly triangular, naked in the intact animal; proximal edge convex; distal edge unequally convex; adradial edge irregular, slightly convex in the middle; abradial edge with two well-defined processes, distal prominent (Fig. 9A–B). Externally, distal half swollen, with a raised oval in the center corresponding to the naked section in the intact animal; oval surface surrounded by numerous small pores; scattered larger pores placed near edges and proximal section (Fig. 9A). Internally, distal half center with three median pores; close to distal edge, two rounded truncated bulbs slightly separated, adradial one larger, followed by a furrow (Fig. 9B). Dental plate fragmented into several pieces (up to

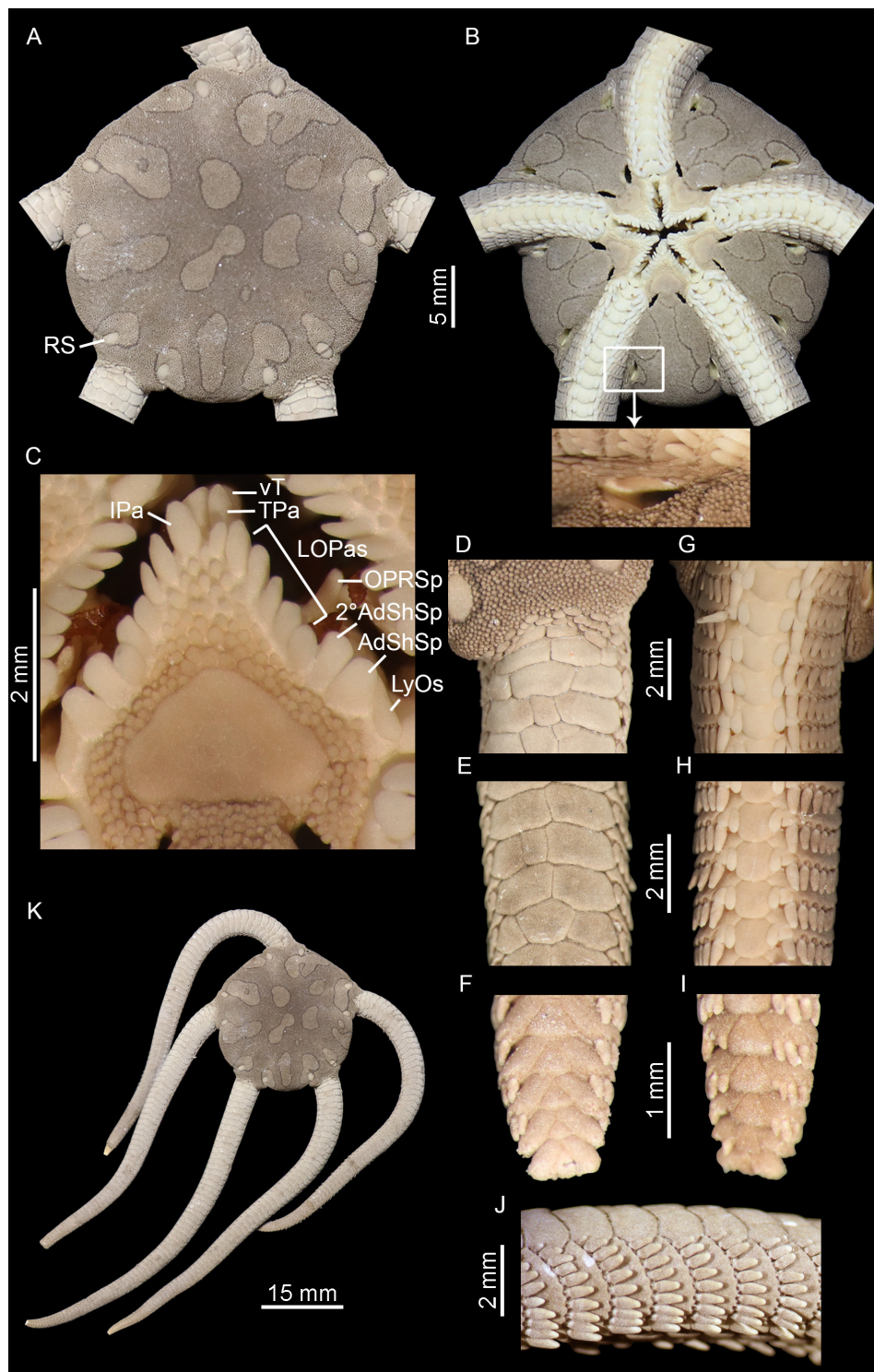


Fig. 8. *Ophioderma aija* sp. nov., holotype (ICML-UNAM 18466, DD = 26.7 mm). **A.** Dorsal disc. **B.** Ventral disc (inset: section between the arm and the distal genital slit). **C.** Close-up of a jaw. **D.** Proximalmost dorsal arm. **E.** Median dorsal arm. **F.** Distalmost dorsal arm. **G.** Proximalmost ventral arm. **H.** Median ventral arm. **I.** Distalmost ventral arm. **J.** Lateral arm plates and arm spines. **K.** Dorsal view. Abbreviations: 2° AdShSp = secondary adoral shield spine; AdShSp = adoral shield spine; IPa = infradental papilla; LOPas = lateral oral papillae; LyOs = Lyman's ossicle; OPRSp = oral plate ridge spine; RS = radial shield; TPa = tooth papilla; vT = ventralmost tooth.

five), bearing one or two teeth in oval or round non-penetrating sockets; ventralmost piece also with round sockets for TPa (Fig. 9C). Adradial genital plate falcate, elongated. Abradial face slightly depressed in the middle, longitudinally, with three pores close to distal edge; distal edge with two truncated knobs and a distal depression, noticed from the other side (Fig. 9D). Adradial face with a longitudinal groove and a notorious pore close to distal section. Distal edge rounded, with a lateral depression followed by a knob (Fig. 9E). Oral plates longer than high, middle section slightly lower than ends (Fig. 9F–G); abradial face with muscle fossa irregularly oval, elongated (Fig. 9F); adradial face with multiple pores at proximoventral edge of plate corresponding to oral papillae (lateral) and granules (ventral) sockets (Fig. 9G). Vertebrae zygospondylus (Fig. 9H–I). Proximal vertebrae wider than long, with dorsal muscle fossae larger than ventral ones (Fig. 9H). VAPs (from proximal arm section) quadrangular, longer than wide; proximal edge with three points, the median one corresponding to a spur; lateral edges with two points forming concave areas; distal edge convex (Fig. 9J). Internal face with three spurs, two elongated and lateral, and one smaller, oval in the middle (Fig. 9K). LAPs curved, 2 × as high as wide; dorsal edge straight; ventral edge convex, with a small, rounded condyle developing from internal side; proximal edge concave; distal edge convex (Fig. 9L–N). Proximal external LAP edge with two conspicuous, elongated, and triangular spurs in the middle (Fig. 9L), having their counterparts internally (Fig. 9M). Internal side with four pores near center, concave proximal ridge, two separated bulbs near ventral edge, ventralmost protruding from plate. Ten spine articulations on distal edge, each surrounded by a thick lobe (Fig. 9N).

Paratype and non-type variations

Paratypes varied in size from 3.6 to 23.7 mm (DD). The two smallest specimens (DD = 3.6 and 4.8 mm) showed radial shields, jaws (including oral shields), DAPs, VAPs, and LAPs covered with granules, as well as the arm base and the section between the arm and distal genital slit. The arm spines in these specimens were up to five, short and pointed. Larger specimens (DD = 9.4–23.7 mm) resembled more the holotype, as they had naked radial shields, oral shields and arms without granules, and scales on the arm base and distal genital slit. These presented exposed DAPs, divided into a maximum of three pieces in the smallest specimen (DD = 9.4 mm) and seven in larger ones (DD > 22.4 mm), varying according to size. The maximum number of arm spines also varied with size, ranging from seven (DD = 9.4 mm) to nine (DD = 17.2–23.7 mm). As for coloration, all paratypes exhibited dark, sinuous rings on the disc. The number and color intensity of these rings varied within (dorsal/ventral sides) and between specimens. The smallest specimens showed the faintest rings, which were quite susceptible to fading with preservation. Paratypes presented light brown, dark brown, or cream-colored oral shields with a brown center. On the ventral side, the interradii were as dark as the disc or light, darkening towards the disc edge.

Other variations were observed in non-type specimens (DD = 6.0–26.4 mm). As in the paratypes, the smallest specimens (DD < 8.5 mm) had radial shields covered with granules; however, two large specimens (DD = 18.8 and 23.6 mm) also presented covered radial shields. Four specimens (DD = 10.6–19.0 mm) had one to several small, rounded plates on the disc. A few specimens showed trilobed, rather than rounded triangular, oral shields. Specimens with DD from 5.6 mm began to show some uncovered DAPs in the proximal and median arm sections, mostly entire or divided into up to two pieces, while their VAPs, LAPs, and oral shields remained covered. On the other hand, those with DD from 7.7 mm had all their DAPs, VAPs, LAPs, and oral shields without granules. In terms of coloration, one specimen presented a uniform light brown ventral side, and another had a general cream coloration with dark, sinuous rings on the dorsal disc.

Distribution and habitat

Ophioderma aija sp. nov. has been collected in Mexico in the Gulf of California (Sonora, Baja California Sur), Jalisco, Colima, Michoacán, Guerrero, and Oaxaca, as well as in Nicaragua, in Cardon Island (see

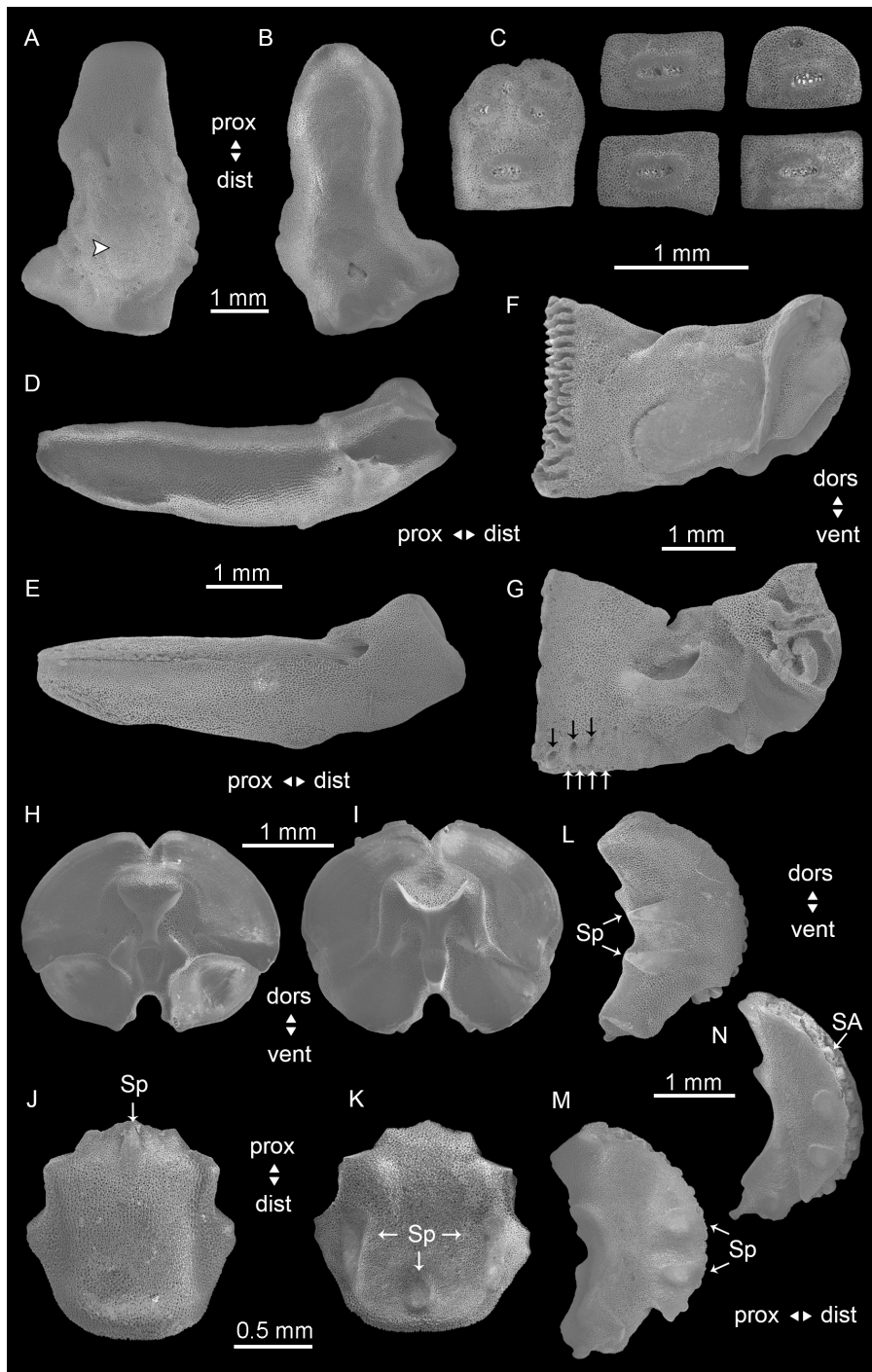


Fig. 9. *Ophioderma aija* sp. nov., non-type specimen (ICML-UNAM 18457, DD = 26.2 mm), SEM images of the ossicles. **A.** Radial shield, external face. The arrowhead indicates the naked section observed in the intact animal. **B.** Radial shield, internal face. **C.** Dental plate. **D.** Adradial genital plate, abradial face. **E.** Adradial genital plate, adradial face. **F.** Oral plate, abradial face. **G.** Oral plate, adradial face. Black arrows point to oral papillae sockets, white arrows point to granule sockets. **H.** Arm vertebra, proximal face. **I.** Arm vertebra, distal face. **J.** Ventral arm plate, external face. **K.** Ventral arm plate, internal face. **L.** Lateral arm plate, external face. **M.** Lateral arm plate, internal face. **N.** Lateral arm plate, lateral face. Abbreviations: dist = distal; dors = dorsal; prox = proximal; SA = spine articulation; Sp = spur; vent = ventral.

[Supp. file 1](#)). Its northernmost record is from Guaymas, Sonora, Mexico (27° N), and the southernmost from Cardon Island, Corinto, Nicaragua (12° N) (Fig. 5). The species may also occur in Ecuador (Galapagos Islands and La Plata), according to Ziesenhenné (1955: 191). Revising material from these areas would help to confirm this. *Ophioderma aija* is found typically on rocks, but also on shingle, sand, and live and dead coral, from the intertidal zone to 27 m depth.

Remarks

Despite being recorded since 1860 (Lyman 1860), *O. aija* sp. nov. remained undescribed due to its misidentification as either *O. teres* or *O. unicolor* stat. nov. Confusion with *O. teres* arose from the original description of this species, where Lyman (1860: 258) included a specimen of *O. aija* (DD = 14 mm) as additional material, describing its characteristic color pattern: "...very dark umber, with fine, sinuous, black lines on the disc". Since then, *O. aija* has been recorded as *O. teres* by other authors (e.g., Lyman 1865; Steinbeck & Ricketts 1941; Caso 1951; Granja-Fernández & López-Pérez 2011), occasionally attributing their morphological differences to distribution, habitat (Ziesenhenné 1955), or a juvenile life stage (Granja-Fernández *et al.* 2014). On the other hand, the misidentification as *O. unicolor* started due to a mixture of one specimen of *O. aija* in the type series of *O. unicolor* (H.L. Clark 1940; Downey 1969). Revision of the former paratype (MCZ IZ OPH-167471) led some authors to identify *O. aija* as *O. teres* var. *unicolor* (Granja-Fernández 2019; Mireles-Velázquez *et al.* 2021) or *O. cf. teres unicolor* (Humara-Gil *et al.* 2022). In this work, the comprehensive revision of the type series of *O. unicolor* resulted in the reclassification of the specimen of *O. aija* as a distinct species.

Ophioderma aija sp. nov. shares with *O. teres* and *O. unicolor* stat. nov. the covered adoral shields and divided DAPs. However, they differ as follows: 1) radial shields typically naked in *O. aija* and *O. unicolor* versus radial shields either covered or naked in *O. teres*; 2) shorter arms in *O. aija* (mean AL:DD = 2.7) than in *O. teres* (mean AL:DD = 4.1) and *O. unicolor* (mean AL:DD = 3.6); 3) DAPs divided into more pieces in *O. aija* (mean = 3, maximum = 9) and *O. teres* (mean = 3, maximum = 13) than in *O. unicolor* (mean = 2, maximum = 6), and 4) color pattern with dark, sinuous rings in the disc in *O. aija*, rounded cream specks in the disc and arms in *O. teres*, and uniform brown disc and arms in *O. unicolor*.

As mentioned previously, one of the most distinctive characters of *O. aija* sp. nov. is its color pattern. Although the rings remain visible in preserved specimens as old as 163 years (MZC IZ OPH-112), they may fade due to fixation. It is advisable to photograph or label specimens appropriately in the field to avoid confusion with other similar species in case the rings fade. This is particularly important for juvenile specimens whose other diagnostic characters may not be developed.

Ophioderma bichi sp. nov.

[urn:lsid:zoobank.org:act:940B392E-8B70-408E-B306-142FC197D164](https://zoobank.org/urn:lsid:zoobank.org:act:940B392E-8B70-408E-B306-142FC197D164)

Figs 1–2, 5, 10–11, 12C; Tables 1–4

Ophioderma teres – Steinbeck & Ricketts 1941: 391–392 (partim, non Lyman, 1860). — Ziesenhenné 1955: 190 (partim, non Lyman, 1860). — Brusca & Smith 1973: 318–319, figs 12.13–12.14 (partim, non Lyman, 1860). — Brusca 1980: 407, fig. 26.14a–b (partim, non Lyman, 1860). — Granja-Fernández 2019: 273–275 (partim, non Lyman, 1860).

Ophioderma sp. B – This study: 3–12, Figs 1–2, Tables 1–4.

Diagnosis

Radial shields covered with granules. Section between arm and distal genital slits with granule-bearing scales only. DAPs divided into multiple pieces (mean = 2, maximum = 9). Coloration uniform brown dorsally (preserved specimens).

Etymology

The species name *bichi* derives from the Sonoran lexicon, particularly the Cahita language, and means ‘naked’. *Ophioderma bichi* sp. nov. is typically uniform brown (DD > 11.0 mm), giving it a ‘naked’ appearance compared to its EP congeners, most of which display brilliant colors (e.g., *O. panamense*, *O. variegatum*) or distinctive disc and arm patterns (e.g., *O. occultum*, *O. teres*) (Granja-Fernández *et al.* 2020; Humara-Gil *et al.* 2022). The specific epithet corresponds to a Sonoran word since the holotype was collected in Sonora, Mexico.

Material examined

Holotype

MEXICO • dry preserved specimen; Gulf of California, Sonora, Tucson Beach; 31°20′48″ N, 113°38′30″ W; 18 Jan. 1969; B. Burch leg.; USNM E23455.

Paratypes

MEXICO – Sonora • 2 specs (preserved dry); Gulf of California, Choya Bay, Tucson Beach; 5 Nov. 1967; B. Burch leg.; tide pools; USNM E23397 • 1 spec.; same data as for holotype; USNM 1698589 • 1 spec. (preserved in 96% ethanol); Gulf of California, Puerto Peñasco; 31°20′8.03″ N, 113°38′5.88″ W; 2 Oct. 2015; D. Paz leg.; GenBank: OR789592 (COI), OR800004 (16S); ICML-UNAM 18488.

Other material

See [Supp. file 1](#).

Description

Holotype

DD = 33.2 mm, AL = 127.5 mm, AL:DD = 3.8. Disc rounded, covered by rounded granules, slightly separated from each other. Granule size increasing from center to periphery. Some granules rubbed off near disc center, leaving scales visible. Dorsal disc granule density 54 per mm². Radial shields covered by granules. Eleven small plates visible near disc edge (Fig. 10A). Ventral interradii covered with small granules separated from each other; those closer to genital slits, larger. Four genital slits per interradius. Proximal genital slits oval, separated from distal section of oral shields by one or two rows of granules, but in contact with 1st LAP, reaching up to proximal section of 2nd VAP. Distal genital slits oval, slightly longer than proximal ones, placed between 7th and 9th arm segments; surrounded only by granule-bearing scales (Fig. 10B).

Oral shields 1.5 × as wide as long, trilobed; proximal edge convex forming a rounded apex; rounded lateral edges; distal edge convex. Madreporite rounded triangular, with a central depression deviated towards distal section; distal edge convex. Adoral shields covered by granules, separated from each other. Jaws with 8–10 oral papillae: LyOs the largest, 3 × as long as wide, angled upwards; AdShSp rounded quadrangular, robust; 2°AdShSp smaller than AdShSp, rounded rectangular; LOPas 3–5, rectangular to conical, pointed; IPa similar to LOPas, more robust; TPa two at jaw apex, triangular to rectangular, robust. Teeth five: vT rounded rectangular; median teeth quadrangular to triangular; dorsalmost triangular and pointed. OPRSp not evident due to closed mouth. Oral plates covered with granules larger than those covering adoral shields, decreasing in size towards periphery (Fig. 10C).

Five arms rounded, tapering distally: one almost complete, four regenerating close to tip (Fig. 10K). Dorsal arm base with some small scales and few granules scattered between them (Fig. 10D). DAPs wider than long, typically divided into four and up to eight irregular pieces (Fig. 10D–E). DAP pieces sequence of the longest arm: first ten segments, 4, 8, 6, 8, 7, 5, 6, 5, 5, 6; 11th–20th, 4–8; 21st–30th, 4–6; 31st–40th, 4–7; 41st–50th, 3–5; 51st–60th, 3–7; 61st–70th, 3–5; 71st–80th, 2–4; 81st–90th, 1–2; 91st–100th, 1–2; 101st–104th, 1. Distalmost DAPs trapezoidal to triangular, entire (Fig. 10F). First VAP small, 2 × as

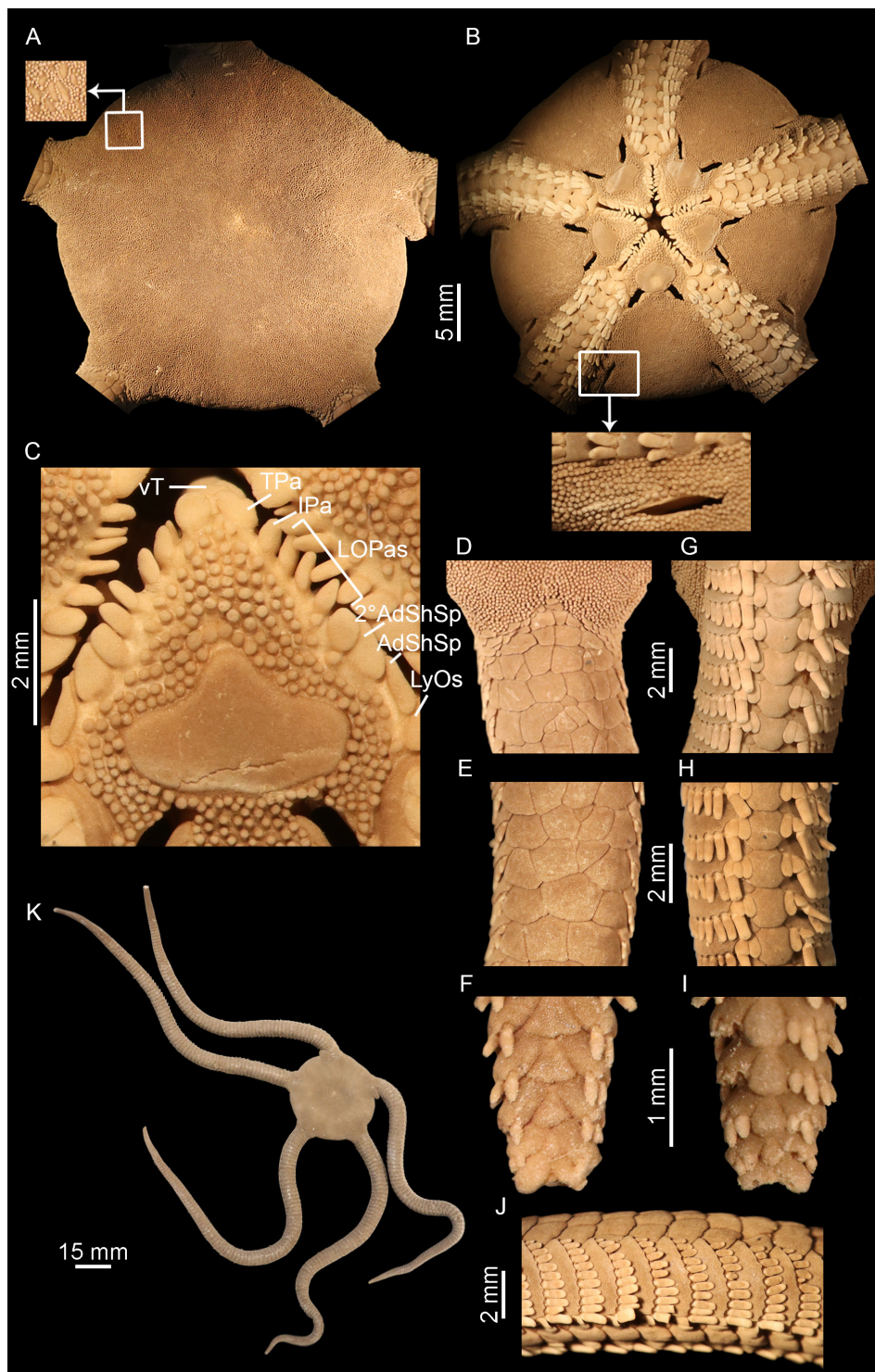


Fig. 10. *Ophioderma bichi* sp. nov., holotype (USNM E23455, DD = 33.2 mm). **A.** Dorsal disc (inset: extra plates on the disc). **B.** Ventral disc (inset: section between the arm and the distal genital slit). **C.** Close-up of a jaw. **D.** Proximalmost dorsal arm. **E.** Median dorsal arm. **F.** Distalmost dorsal arm. **G.** Proximalmost ventral arm. **H.** Median ventral arm. **I.** Distalmost ventral arm. **J.** Lateral arm plates and arm spines. **K.** Dorsal view. Abbreviations: 2° AdShSp = secondary adoral shield spine; AdShSp = adoral shield spine; IPa = infradental papilla; LOPas = lateral oral papillae; LyOs = Lyman's ossicle; TPa = tooth papilla; vT = ventralmost tooth.

wide as long, with rounded edges (Fig. 10B). Subsequent VAPs quadrangular, longer than wide; distal edge convex (Fig. 10G–H). Distalmost VAPs triangular, rounded, slightly longer than wide (Fig. 10I). A pair of pores between the four proximalmost VAPs in all five arms (Fig. 10B). LAPs conspicuous, wider than long, with up to 11 arm spines. Arm spine sequence of the longest arm (right side, including arm spine bearing segments within disc): first ten segments, 2, 2, 3, 4, 4, 6, 6, 7, 8, 10; 11th–20th, 10–11; 21st–30th, 10–11; 31st–40th, 8–11; 41st–50th, 9–10; 51st–60th, 9; 61st–70th, 8–9; 71st–80th, 7–8; 81st–90th, 7–8; 91st–100th, 6–7; 101st–110th, 4–6; 111st–112nd, 3. Arm spines conical with blunt tips, slightly flattened, $\frac{2}{3}$ LAP length. Dorsalmost arm spine the shortest; ventralmost the longest and more robust, in contact with tentacle scales of the following segment (Fig. 10J). Two tentacle scales, rarely three; adradial tentacle scale oval, elongated, $\frac{2}{3}$ VAP length; abradial tentacle scale shorter, $\frac{3}{4}$ adradial scale length, triangular (Fig. 10G–H). In the distalmost arm section, tentacle scales oval and elongated, adradial being the longest; last arm segments with only one scale (Fig. 10I).

General coloration uniform brown (dry specimen) (Fig. 10K). Dorsal side: disc brown (Fig. 10A). Arms brown (Fig. 10D–F, K). Ventral side: interradial brown (Fig. 10B). Oral shields brown; oral papillae and teeth cream (Fig. 10B–C). LAPs brown. Arm spines brown with cream bases and tips; the ventralmost, cream (Fig. 10J).

Disarticulated ossicles

Non-type specimen, USNM E23396 (DD = 28.1 mm, AL = 111.9 mm, AL:DD = 3.9). Radial shields irregularly triangular, elongated, covered in the intact animal; proximal edge convex; distal edge convex; adradial edge irregular with a median process; abradial edge with two processes, proximal subtle, distal prominent (Fig. 11A–B). Externally, distal half with swollen center showing multiple small pores, close to each other; additional larger pores closer to edges, proximalmost the largest (Fig. 11A). Internally, distal half center with three small middle pores; distal edge showing two rounded truncated bulbs, adradial one larger, separated by a furrow that continues to distal edge of shield (Fig. 11B). Dental plate fragmented into several pieces (up to five), each supporting one or two teeth in oval or round non-penetrating sockets; ventralmost piece also with round sockets for TPa (Fig. 11C). Adradial genital plate falcate, elongated, proximally curved. Abradial face with a short proximal furrow and two small pores close to distal edge; distal edge with two truncated knobs separated by a furrow, and a distal depression, noticed from the other side (Fig. 11D). Adradial face with a longitudinal groove and a notorious pore close to distal section. Distal edge rounded, laterally showing a depression followed by a central knob (Fig. 11E). Oral plates longer than high, middle section slightly lower than ends (Fig. 11F–G); abradial face with muscle fossa widening ventrally (Fig. 11F); adradial face with multiple pores at proximoventral edge of plate corresponding to oral papillae (lateral) and granule (ventral) sockets (Fig. 11G). Vertebrae zygospondylus (Fig. 11H–I). Proximal vertebrae wider than long, with dorsal muscle fossae larger than ventral ones (Fig. 11H). VAPs (from proximal arm section) quadrangular, slightly wider than long; proximal edge slightly concave, with a median spur; lateral edges with two points forming concave areas; distal edge convex (Fig. 11J). Internal face with two elongated lateral spurs, and a smaller, oval one in the middle (Fig. 11K). LAPs curved, $3 \times$ as high as wide; dorsal edge slightly concave; ventral edge slightly convex, with a small, rounded condyle developing from internal side; proximal edge concave; distal edge convex (Fig. 11L–N). Proximal external LAP edge with two conspicuous, elongated, and triangular spurs in the middle (Fig. 11L), having their counterparts internally (Fig. 11M). Internal side with four pores near center, concave proximal ridge, and two separated bulbs near ventral edge, ventralmost protruding from plate (Fig. 11M). Ten spine articulations on distal edge, each surrounded by a thick lobe (Fig. 11N).

Paratype and non-type variations

Paratypes varied in size from 15.4 to 25.4 mm (DD). The smallest specimens (DD = 15.4 and 19.5 mm) did not show plates on the disc, whereas larger ones presented various irregular plates (DD = 24.1 mm)

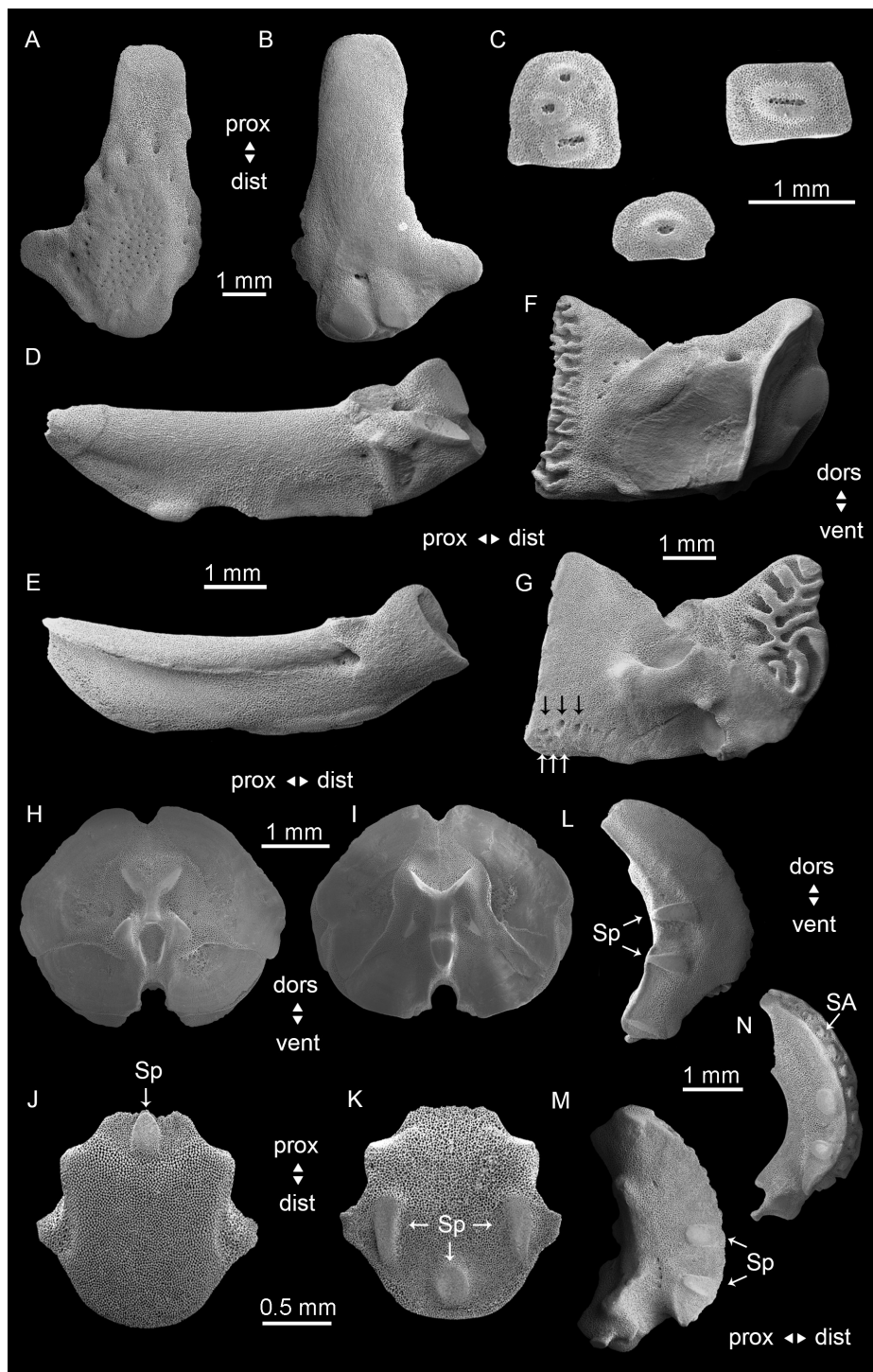


Fig. 11. *Ophioderma bichi* sp. nov., non-type specimen (USNM E23396, DD = 28.1 mm), SEM images of the ossicles. **A.** Radial shield, external face. **B.** Radial shield, internal face. **C.** Dental plate. **D.** Adradial genital plate, abradial face. **E.** Adradial genital plate, adradial face. **F.** Oral plate, abradial face. **G.** Oral plate, adradial face. Black arrows point to oral papillae sockets, white arrows point to granule sockets. **H.** Arm vertebra, proximal face. **I.** Arm vertebra, distal face. **J.** Ventral arm plate, external face. **K.** Ventral arm plate, internal face. **L.** Lateral arm plate, external face. **M.** Lateral arm plate, internal face. **N.** Lateral arm plate, lateral face. Abbreviations: dist = distal; dors = dorsal; prox = proximal; SA = spine articulation; Sp = spur; vent = ventral.

or a single plate near the arm base (DD = 25.4 mm). Three specimens (DD = 15.4, 19.5, and 24.1 mm) had rounded triangular rather than trilobed oral shields. All paratypes presented DAPs divided mainly into two pieces, although the maximum number of pieces reached varied with size, being three in the smallest (DD = 15.4 mm) and five in the largest (DD = 25.4 mm). The maximum number of arm spines also varied with size, ranging from nine (DD = 15.4 mm) to 12 (DD = 25.4 mm). In two specimens (DD = 24.1 and 25.4 mm), a few segments had three tentacle scales, while in the remaining two, all segments had two scales. Regarding coloration, one specimen presented some groups of light granules on the dorsal disc; two had arms slightly lighter than the disc, and another showed a small, cream speck on the distal section of each oral shield, except for the madreporite.

Other variations were observed in non-type specimens (DD = 8.5–32.9 mm). Two specimens had one radial shield partially naked. Seven of the smallest specimens (DD = 8.5–11.9 mm) presented mostly entire DAPs along the arm. Additionally, 18 specimens showed clusters of light granules on the ventral disc, ranging from a few to several. These were mainly present in specimens with DD = 8.5 to 11.0 mm but were also observed in larger ones with DD up to 19.5 mm.

Distribution and habitat

Ophioderma bichi sp. nov. is exclusively found in the northern Mexican Pacific waters, specifically in the Gulf of California (Baja California, Sonora, and Baja California Sur) and Revillagigedo Islands (Roca Partida Island). The northernmost record of this species corresponds to Punta Pelicano, Sonora (31° N), and the southernmost to Bahía Eclipse, Roca Partida Island (19° N) (Fig. 5). *Ophioderma bichi* inhabits rocky substrate, shingle, and sediment under rocks and can be found from intertidal to 12 m depth. This is the third species of *Ophioderma*, alongside *O. occultum* and *O. vansyoci*, with a restricted distribution in the northern Mexican Pacific (Hendler 1996; Hernández-Herrejón *et al.* 2010; Humara-Gil *et al.* 2022).

Remarks

Ophioderma bichi sp. nov. is another species that was previously ‘hidden’ within *O. teres*. Material of this new species in scientific collections dates back to 1888, but it was often identified as *O. teres* (Steinbeck & Ricketts 1941; Ziesenhenné 1955; Brusca & Smith 1973; Brusca 1980; Granja-Fernández 2019). Remarkably, Ziesenhenné (1955: 190) noted that certain “uniform brown” specimens from the northern Mexican Pacific did not match Lyman’s (1860) description of *O. teres*; still, he interpreted the differences as intraspecific variations. Those specimens belonged to *O. bichi*.

Ophioderma bichi sp. nov. resembles *O. teres* in having covered adoral shields and divided DAPs. However, they differ in the following characters: 1) radial shields always covered in *O. bichi* versus radial shields either covered or naked in *O. teres*; 2) section between the arm and distal genital slits only with granule-bearing scales in *O. bichi*, and with naked and granule-bearing scales in *O. teres*; 3) coloration uniform brown in *O. bichi* versus disc and arms brown speckled with cream in *O. teres*; and 4) *O. bichi* is distributed in the northern Mexican Pacific, and *O. teres* is mainly found on the Pacific coast of Central America.

Other species with which *O. bichi* sp. nov. might be mistaken are *O. occultum* and *O. unicolor* stat. nov. In the collections, *O. bichi* was frequently found alongside *O. occultum*, although in lower abundance: a specimen of *O. bichi* for every 2–46 specimens of *O. occultum*. These species share their covered radial and adoral shields, divided DAPs, and are distributed in the same areas (Gulf of California and Revillagigedo Islands). Nevertheless, they differ in two important characters: 1) *O. bichi* only presents granule-bearing scales in the section between the arm and the distal genital slits, while *O. occultum* presents naked and granule-bearing scales, and 2) *O. bichi* presents a uniform brown coloration, while *O. occultum* has banded arms and paired white blotches in the median and distal arm sections (Humara-

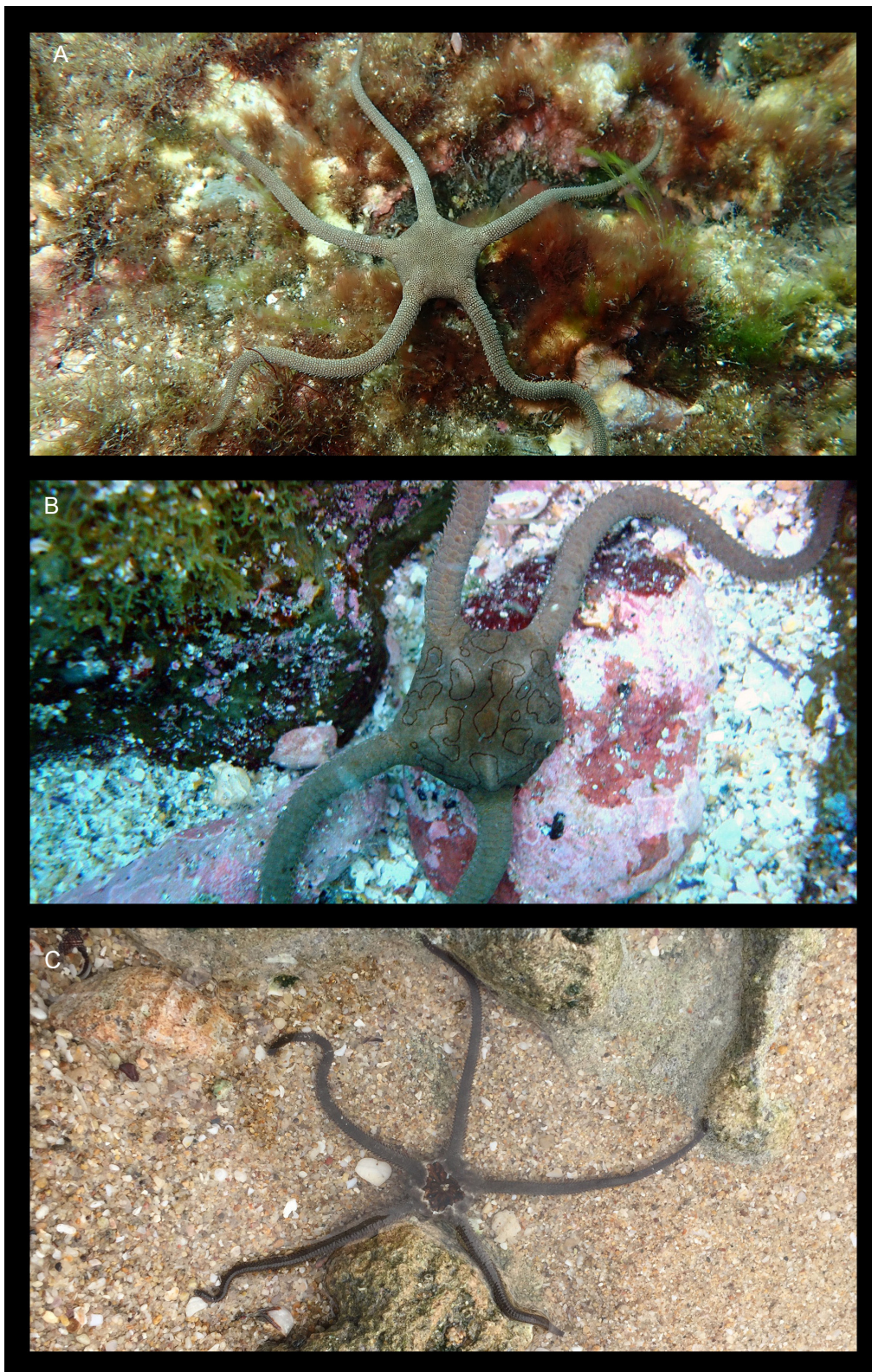


Fig. 12. Photographs of the species in situ. **A.** *Ophioderma teres* (Lyman, 1860) (Bajo Rojo, Costa Rica) (photograph: Steven Lara-Angulo). **B.** *Ophioderma aija* sp. nov. (Estacahuite, Mexico) (photograph: Francisco Benítez-Villalobos). **C.** *Ophioderma bichi* sp. nov. (Puerto Peñasco, Mexico) (photograph: Paloma Valdivia).

Gil *et al.* 2022). These characters can change in young specimens, making their differentiation difficult. In such cases, the most reliable character to differentiate both is the banding in the arms of *O. occultum*, which is never present in *O. bichi* (Humara-Gil *et al.* 2022). Regarding the confusion between *O. bichi* and *O. unicolor*, the differences between both are indicated above (see *O. unicolor* Remarks).

A relevant variation in *O. bichi* sp. nov. was observed in its coloration. Although all but one specimen had a uniform brown coloration on the dorsal side, there were differences in the ventral coloration of the disc, which could be either uniform brown (n = 36) or with clusters of white granules (n = 18). This variation appears to be associated with age, as younger (= smaller) specimens exhibited white granules more frequently (see Paratype and non-type variations). An age-related coloration in *O. bichi* would not be uncommon, as changes in the coloration of juveniles have been documented in other species of *Ophioderma*, such as *O. cinereum*, *O. occultum*, and *O. panamense* (Hendler *et al.* 1995; Granja-Fernández *et al.* 2014; Humara-Gil *et al.* 2022). Further investigation of *O. bichi* specimens of various sizes is necessary to corroborate whether this variation is indeed related to the developmental stage.

Key to the eastern Pacific species of *Ophioderma*

This key serves as a reference for the identification of valid nominal species of *Ophioderma* in the EP. Before use, the following should be considered: 1) possible new undescribed species have been reported in the region, particularly in California, Baja California (Pacific side), and Clipperton Island (Lessios & Hendler 2022). Caution should be used when employing this key to identify specimens from these locations; 2) some diagnostic characters vary according to size (e.g., granulation extent, fragmentation of DAPs, number of arm spines) (Granja-Fernández *et al.* 2020; Stöhr *et al.* 2020; Humara-Gil *et al.* 2022). Therefore, small individuals (= younger) may not have developed all the characters included in the key.

1. Disc covered with flattened, brick-like granules *O. vansyoci* Hendler, 1996
 – Disc covered with rounded granules 2
2. Dorsal arm plates mostly or always entire 3
 – Dorsal arm plates fragmented into two or more pieces 6
3. Dorsal arm plates mostly entire; a few can be divided into up to two pieces. Radial shields naked. Adoral shields covered with granules. Arms with transverse bands (in vivo and preserved)
 *O. panamense* Lütken, 1859
 – Dorsal arm plates entire. Radial shields covered with granules. Adoral shields naked 4
4. Distal genital slit with granule-bearing scales only. Disc olive green with dark pink or red (in vivo), or light brown (preserved); arms with olive green and dark pink/red (in vivo) or dark brown transverse bands (preserved) *O. variegatum* Lütken, 1856
 – Distal genital slit with naked and granule-bearing scales. Disc brown (preserved); arms with transverse bands (in vivo and preserved) 5
5. Disc dark brown with small white spots. Up to 11 arm spines
 *O. hendleri* Granja-Fernández *et al.*, 2020
 – Disc orange (in vivo) or brown (preserved), with dark blotches. Up to six arm spines
 *O. pentacanthum* H.L. Clark, 1917
6. Coloration uniform brown on disc and arms 7
 – Coloration with characteristic patterns on disc or arms 8

7. Distal genital slit with granule-bearing scales only *O. bichi* sp. nov.
 – Distal genital slit with naked and granule-bearing scales *O. unicolor* H.L. Clark, 1940 stat. nov.
8. Disc dark olive green to brown (in vivo), or dark gray to brown (preserved); arms with transverse bands (more subtle in preserved specimens) and parallel white bands in the median and distal arm sections *O. occultum* Humara-Gil *et al.*, 2022
 – Disc with specks or rings; arms without bands 9
9. Disc dark brown with darker, sinuous rings on both dorsal and ventral sides. Radial shields naked *O. aija* sp. nov.
 – Disc speckled. Radial shields covered or naked 10
10. Granules present on the disc and the distal part of dorsal arm plates in the proximalmost and median arm sections *O. peruanum* Pineda-Enríquez *et al.*, 2013
 – Granules limited to the disc and arm base *O. teres* (Lyman, 1860)

Discussion

Until 2022, the genus *Ophioderma* in the EP consisted of nine species and one subspecies with an uncertain taxonomic status (Humara-Gil *et al.* 2022). With the newly proposed additions and amendments within the genus, this count has increased to eleven valid species. Worldwide, *Ophioderma* currently numbers 35 species (Stöhr *et al.* 2023b).

In this study, the use of morphological, morphometric, and molecular data allowed to clarify the taxonomic status of the *O. teres*-like species: *O. teres*, *O. sodipallaresi* (= *O. teres*), *O. unicolor* stat. nov., *O. aija* sp. nov., and *O. bichi* sp. nov. Morphologically, external characters such as covered or naked radial shields, distal genital slit ornamentation, and color pattern, as well as internal characters like the shape of the radial shields and oral plates, were diagnostic at the species level, as demonstrated in previous works on other *Ophioderma* (Granja-Fernández *et al.* 2020; Stöhr *et al.* 2020; Humara-Gil *et al.* 2022). These characters, although diagnostic, may show intraspecific variation related to the size of the specimens examined (see Paratype and non-type variations), particularly in juveniles. Therefore, young *Ophioderma* must be carefully examined to avoid misidentification, and if possible, their identification should be complemented with DNA analysis. Among the diagnostic morphological characters, one that deserves mention is the color pattern. For years the taxonomic relevance of this character in *Ophioderma* was neglected under the assumption that it typically showed great variation within the same species (Ziesenhenne 1955). However, recent works on the genus, including this study, have challenged this opinion, demonstrating that the color variants within *Ophioderma longicaudum* (Bruzelius, 1805), *O. panamense*, *O. teres*, and *O. variegatum* represent different species, all showing other recognizable morphological variations as well (Granja-Fernández *et al.* 2020; Stöhr *et al.* 2020; Humara-Gil *et al.* 2022). The extent to which color pattern varies, through development, for example, or in species from other geographic areas should be further investigated.

Regarding morphometrics, the number of LOPas, the number of DAP pieces, the length:width ratio of the median VAP, and the number of arm spines were the variables that contributed the most to the differentiation between these species. Some of these characters are now incorporated into the diagnoses of the species. It is important to highlight that all measurements were obtained from intact animals. This is especially practical when samples for skeletal disarticulation are limited or unavailable, for example, in the case of type material. However, it may also be disadvantageous because structures in intact animals have a certain degree of overlap (e.g., DAPs, VAPs), which may influence the accuracy of the measurements and how consistently they are obtained. A comparison of measurements obtained from intact versus disarticulated ossicles is necessary to assess the variation and error rates that one

shows relative to the other. Furthermore, as recommended in the study of the internal morphology of brittle stars (Stöhr *et al.* 2020), it is also worth noting the relevance of including specimens of similar sizes of each species studied in the morphometric analyses. This ensures the comparability of the groups and, if differences are observed, that inherent size changes of the specimens do not influence them.

Lastly, molecular data also supported the delimitation of the species with available sequences (*O. aija* sp. nov., *O. bichi* sp. nov., and *O. teres*) showing mean genetic distances (COI: 3.3–8.6%; 16S: 6.1%) within the ranges considered as interspecific variation in *Ophioderma* (COI: 2.2–10.2%; 16S: >3%) (Boissin *et al.* 2011; Humara-Gil *et al.* 2022). Although it was not possible to obtain all data from each species due to a lack of suitable material or a limited number of specimens, applying the consensus protocol for integrative taxonomy (Padial *et al.* 2010), which combines the advantages of integration by cumulation and congruence, validated the results found.

Geography was not evaluated in this study as additional evidence to differentiate *O. teres* from its similar congeners. However, it appears informative, as in other *Ophioderma* (Stöhr *et al.* 2020; Humara-Gil *et al.* 2022). So far, records of the species suggest that each of them follows a particular pattern in terms of distribution. From north to south: *Ophioderma bichi* sp. nov. shows a restricted distribution to the Gulf of California and Revillagigedo Islands; *O. aija* sp. nov. has been found from the Gulf of California to Nicaragua, with most of its records corresponding to the tropical Mexican Pacific; *O. teres* has been mainly recorded from Central America, with sporadic records in Mexico and Colombia, and finally, *O. unicolor* stat. nov., is mainly present in the Galapagos Islands, with an additional record from Nicaragua (Fig. 5). Future specialized analyses, including new geographic information from other museum collections and fieldwork, will help to corroborate these observations.

In the last years, the taxonomy of EP *Ophioderma* has been addressed and resolved (Granja-Fernández *et al.* 2020; Humara-Gil *et al.* 2022; this study). However, there are still problems to be dealt with, including the elucidation of the identity of *O. panamense*, which apparently comprises multiple species (Varela-Sánchez *et al.* 2020; Lessios & Hendler 2022), or the validity of *O. peruanum* and its relation to *O. teres*. These issues are more likely to be puzzled out through the implementation of integrative approaches, using diverse types of evidence (morphology, DNA, ecology, geography) or methods (qualitative, quantitative).

Finally, the situation observed within a “well-known” species of a common genus in the EP like *Ophioderma* (Granja-Fernández *et al.* 2020), emphasizes the need for further work in Ophiuroidea taxonomy in the region, including both conspicuous and less conspicuous genera.

Acknowledgments

We are indebted to the people who kindly helped us with the logistics before and during visits to the collections: Yuri Hooker (CZA); Mercedes Cordero and Michel Hendrickx (ICML-EMU); Alicia Durán-González, Daniel Mireles-Velázquez, and Carlos Conejeros-Vargas (ICML-UNAM); Gordon Hendler and Cathy Groves (LACM); Adam Baldinger, Rina Morisawa, and Penny Benson (MCZ); Leonardo Chacón-Monge and Juan José Alvarado (MZUCR); Tom Schiøtte and Jørgen Olesen (NHMD); Maria Criales (UMML); and Yolanda Villacampa, Chris Mah, Ellen Strong, Dave Pawson, Chad Walter, Chris Meyer, Karen Reed, Geoff Keel, Jon Norenburg, Paul Greenhall, Phoebe Fu, Scott Whittaker, Tim Coffer, Amanda Robinson, and Freya Goetz (USNM). To Alejandro Hernández-Morales and Marco Medina-López (Universidad Autónoma de Baja California Sur), Brenda Maya-Alvarado (Universidad de Guadalajara (UdeG)), David Paz-García (Centro de Investigaciones Biológicas del Noreste), Sergio Guendulain-García (Universidad Autónoma Metropolitana), Aldo Zavala-Jiménez (University of California, Santa Cruz), Dinorah Herrero-Pérezrul (Centro Interdisciplinario de Ciencias Marinas (CICIMAR)), Emerson Martínez-Zavala, and Diego Rangel-Solís for their help in collecting

specimens. To Itzel Rosales-Contreras and Carlos Conejeros-Vargas (ICML-UNAM) for their advice on SEM preparations. To Berenit Mendoza-Garfias (IBUNAM) for her guidance during the SEM imaging sessions in Mexico. To Hazel Canizales-Flores for introducing the Sonoran lexicon that resulted in the name of *O. bichi* sp. nov. To Steven Lara-Angulo (Diving Center Cuajiniquil), Leonardo Chacón-Monge (MZUCR), Francisco Benítez-Villalobos (Universidad del Mar), and Paloma Valdivia (Centro Intercultural de Estudios de Desiertos y Océanos) for sharing the in situ photographs used in Fig. 12. To Christopher Cruz-Gómez (El Colegio de la Frontera Sur), Brenda Maya-Alvarado (UdeG), and Miriam Hueytletl-Pérez (CICIMAR) for their valuable comments on previous versions of this manuscript. To Renata Alitto (Universidade de São Paulo) and an anonymous reviewer whose insightful suggestions improved the work. Finally, to Didier Van den Spiegel (Royal Museum for Central Africa), Pepe Fernández (Museo Nacional Ciencias Naturales), and Magalie Castelin (Muséum National d'Histoire Naturelle) for their guidance through the editorial process. This work is part of the PhD thesis of KJHG at UdeG and was supported by the Consejo Nacional de Humanidades, Ciencias y Tecnologías (under grant 993677 to KJHG); the Museum of Comparative Zoology (under the Ernst Mayr Travel Grant to KJHG (2020) and RGF (2016)); the Smithsonian Institution (under the Kenneth Jay Boss Fellowship in Invertebrate Zoology to KJHG (2022)); the National Geographic Society (NGS-100354C-23 to APRT); the Plataforma de Movilidad Estudiantil y Académica de la Alianza del Pacífico, Programa Nacional de Becas y Crédito Educativo (PRONABEC-Peru to RGF), and the Comisión Nacional para el Conocimiento y Uso de la Biodiversidad (JF047 to RGF).

References

- Alvarado J.J., Chacón-Monge J.L., Solís-Marín F.A., Pineda-Enríquez T., Caballero-Ochoa A.A., Rivera S.S. & Chaves R.R. 2017. Equinodermos del Museo de Zoología de la Universidad de Costa Rica. *Revista de Biología Tropical* 65 (1): S272–S287. <https://doi.org/10.15517/rbt.v65i1-1.31695>
- Anderson M.J. 2001. A new method for non-parametric multivariate analysis of variance. *Austral Ecology* 26: 32–46. <https://doi.org/10.1111/j.1442-9993.2001.01070.pp.x>
- Boissin E., Stöhr S. & Chenuil A. 2011. Did vicariance and adaptation drive cryptic speciation and evolution of brooding in *Ophioderma longicauda* (Echinodermata: Ophiuroidea), a common Atlanto-Mediterranean ophiuroid? *Molecular Ecology* 2: 4737–4755. <https://doi.org/10.1111/j.1365-294X.2011.05309.x>
- Brusca R.C. 1980. 26. Echinodermata. In: Brusca R.C. (ed.) *Common Intertidal Invertebrates of the Gulf of California*: 398–422. University of Arizona Press, Tucson.
- Brusca R.C. & Smith C.R. 1973. Echinodermata (Starfish, etc.). In: Brusca R.C. (ed.) *A Handbook to the Common Intertidal Invertebrates of the Gulf of California*: 304–343. University of Arizona Press, Tucson.
- Caso M.E. 1951. Contribución al conocimiento de los ofiuroides de México. I. Algunas especies de ofiuroides litorales. *Anales del Instituto de Biología, Universidad Nacional Autónoma de México* 22 (1): 219–312.
- Caso M.E. 1986. Descripción de una nueva especie de ofiuroides de la bahía de Mazatlán, Sin. *Ophioderma sodipallaresi* sp. nov. y comparación con *Ophioderma variegatum* Lütken. *Anales del Instituto de Ciencias del Mar y Limnología, Universidad Nacional Autónoma de México* 13 (2): 223–248.
- Clark H.L. 1940. Eastern Pacific Expeditions of the New York Zoological Society. XXI. Notes on Echinoderms from the west coast of Central America. *Zoologica* 25 (3): 331–352. <https://doi.org/10.5962/p.184708>

- Clarke K.R. 1993. Non-parametric multivariate analyses of changes in community structure. *Australian Journal of Ecology* 18: 117–143. <https://doi.org/10.1111/j.1442-9993.1993.tb00438.x>
- Darriba D., Taboada G.L., Doallo R. & Posada D. 2012. jModelTest2: more models, new heuristic and parallel computing. *Nature Methods* 9: 772. <https://doi.org/10.1038/nmeth.2109>
- Downey M.E. 1969. Catalog of recent ophiuroid type specimens in major collections in the United States. *United States National Museum Bulletin* 293: 1–239. <https://doi.org/10.5479/si.03629236.293>
- Edgar R.C. 2004. MUSCLE: multiple sequence alignment with high accuracy and high throughput. *Nucleic Acids Research* 32 (5): 1792–1797. <https://doi.org/10.1093/nar/gkh340>
- Gondim A.I., Alonso C., Días T.L.P., Manso C.L.C & Christoffersen M.L. 2013. A taxonomic guide to the brittle stars (Echinodermata, Ophiuroidea) from the State of Paraíba continental shelf, Northeastern Brazil. *ZooKeys* 307: 45–96. <https://doi.org/10.3897/zookeys.307.4673>
- Granja-Fernández M.R. 2019. *Ophiuroideos (Echinodermata) del Pacífico oriental tropical*. PhD thesis, Universidad Autónoma Metropolitana, Mexico.
- Granja-Fernández M.R. & López-Pérez R.A. 2011. Nuevos registros de ophiuroideos (Echinodermata: Ophiuroidea) para localidades de Zihuatanejo (Guerrero) y Puerto Escondido (Oaxaca), Pacífico Mexicano. *Revista Mexicana de Biodiversidad* 82: 1320–1323. <https://doi.org/10.22201/ib.20078706e.2011.4.675>
- Granja-Fernández R. & Hooker Y. 2020. Revisiting the diversity and distribution of the ophiuroids (Echinodermata: Ophiuroidea) from Peru. *Zootaxa* 4766: 539–556. <https://doi.org/10.11646/zootaxa.4766.4.2>
- Granja-Fernández R., Herrero-Pérezrul M.D., López-Pérez R.A., Hernández L., Rodríguez-Zaragoza F.A., Jones R.W. & Pineda-López R. 2014. Ophiuroidea (Echinodermata) from coral reefs in the Mexican Pacific. *ZooKeys* 406: 101–145. <https://doi.org/10.3897/zookeys.406.6306>
- Granja-Fernández R., Herrero-Pérezrul M.D., López-Pérez R.A., Hernández-Morales A. & Rangel-Solís P.D. 2015. A literature review of the Ophiuroidea (Echinodermata) from the Pacific coast of Mexico. *Revista de Biología Tropical* 63 (2): 37–47. <https://doi.org/10.15517/rbt.v63i2.23127>
- Granja-Fernández R., Pineda-Enríquez T., Solís-Marín F.A. & Laguarda-Figueras A. 2020. *Ophioderma hendleri* sp. nov. (Echinodermata: Ophiuroidea: Ophiodermatidae) and its congeners from the Eastern Pacific. *European Journal of Taxonomy* 729: 11–41. <https://doi.org/10.5852/ejt.2020.729.1187>
- Granja-Fernández R., Rodríguez-Zaragoza F.A., López-Pérez A. & López-López D.A. 2022. Coral reef ecosystem-associated echinoderms (Echinodermata) at the Southern Mexican Pacific: species richness, distribution, and composition. *Marine Biodiversity* 52: 65. <https://doi.org/10.1007/s12526-022-01305-0>
- Hammer Ø., Harper D.A.T. & Ryan P.D. 2001. PAST: Paleontological statistics software package for education and data analysis. *Palaeontologia Electronica* 4: 1–9.
- Hendler G. 1996. Echinodermata collected at Rocas Alijos. In: Schmieder R.W. (ed.) *Rocas Alijos. Scientific Results from the Cordell Expeditions*: 319–338. Springer, Dordrecht. https://doi.org/10.1007/978-94-017-2917-8_27
- Hendler G. 2018. Armed to the teeth: a new paradigm for the buccal skeleton of brittle stars (Echinodermata: Ophiuroidea). *Contributions in Science* 526: 189–311. <https://doi.org/10.5962/p.324539>
- Hendler G., Miller J.E., Pawson D.L. & Kier P.M. 1995. *Sea Stars, Sea Urchins, and Allies: Echinoderms of Florida and the Caribbean*. Smithsonian Institution Press, Washington.

- Hernández-Herrejón L.A., Solís-Marín F.A. & Laguarda-Figueras A. 2008. Ofiuroideos (Echinodermata: Ophiuroidea) de las aguas mexicanas del golfo de México. *Revista de Biología Tropical* 56 (3): 83–167. <https://doi.org/10.15517/rbt.v56i3.27082>
- Hernández-Herrejón L.A., Solís-Marín F.A., Laguarda-Figueras A. & Pineda-Enríquez T. 2010. First record of *Ophioderma vansyoci* (Echinodermata: Ophiuroidea) in the Gulf of California. *Marine Biodiversity Records* 3: e114. <https://doi.org/10.1017/S1755267210001028>
- Hickman C.P. Jr 1998. *A Field Guide to Sea Stars and Other Echinoderms of Galápagos*. Sugar Spring Press, Lexington, Virginia.
- Hoareau T.B., Boissin E., Paulay G. & Bruggemann J.H. 2013. The Southern Indian Ocean as a potential marine evolutionary hotspot: perspectives from comparative phylogeography of reef brittle-stars. *Journal of Biogeography* 40: 2167–2179. <https://doi.org/10.1111/jbi.12155>
- Honey-Escandón M., Solís-Marín F.A. & Laguarda-Figueras A. 2008. Equinodermos (Echinodermata) del Pacífico Mexicano. *Revista de Biología Tropical* 56 (3): 57–73. <https://doi.org/10.15517/rbt.v56i3.27079>
- Hugall A.F., O’Hara T.D., Hunjan S., Nilsen R. & Moussalli A. 2016. An exon-capture system for the entire class Ophiuroidea. *Molecular Biology and Evolution* 33 (1): 281–294. <https://doi.org/10.1093/molbev/msv216>
- Humara-Gil K.J., Granja-Fernández R., Bautista-Guerrero E. & Rodríguez-Troncoso A.P. 2022. Overlooked for over a century: *Ophioderma occultum* sp. nov. (Echinodermata), a new species of brittle star from the Eastern Pacific. *Journal of Natural History* 56 (5–8): 365–384. <https://doi.org/10.1080/00222933.2022.2071179>
- ICZN (International Commission of Zoological Nomenclature) 1999. *International Code of Zoological Nomenclature, 4th edition*. International Commission on Zoological Nomenclature, London. Available from <https://www.iczn.org/the-code/the-code-online/> [accessed 1 Jul. 2023].
- Lessios H. & Hendler G. 2022. Mitochondrial phylogeny of the brittle star genus *Ophioderma*. *Scientific Reports* 12: 5304. <https://doi.org/10.1038/s41598-022-08944-0>
- Ljungman A. 1867. Ophiuroidea vivencia huc usque cognita enumerat. *Öfversigt af Kongl. Vetenskaps-akademiens forhandlingar* 23 (9): 303–336.
- Lyman T. 1860. Descriptions of new Ophiuridae, belonging to the Smithsonian Institution and to the Museum of Comparative Zoology at Cambridge. *Proceedings of the Boston Society of Natural History* 7: 193–204, 252–262. <https://doi.org/10.5962/bhl.part.4822>
- Lyman T. 1865. Ophiuridae and Astrophytidae. *Illustrated Catalogue of the Museum of Comparative Zoology at Harvard College* 1: 1–200. <https://doi.org/10.5962/bhl.title.40077>
- Maluf L.Y. 1988. *Composition and Distribution of the Central Eastern Pacific Echinoderms*. Technical Report 2, Natural History Museum of Los Angeles County, Los Angeles, California.
- Martinez-Arbizu P. 2017. PairwiseAdonis: Pairwise Multilevel Comparison using Adonis. R package version 0.4.1.
- Mireles-Velázquez D., Rosales-Contreras G.I., Conejeros-Vargas C.A., Solís-Marín F.A. & Granja-Fernández R. 2021. Los ofiuroideos (Echinodermata: Ophiuroidea) de la bahía de Chamela, Jalisco, México. *Revista de Biología Tropical* 69 (S1): 312–333. <https://doi.org/10.15517/rbt.v69iSuppl.1.46364>
- Nielsen E. 1932. Papers from Dr. Th. Mortensen’s Pacific Expedition 1914–1916. LIX. Ophiurans from the Gulf of Panama, California, and the Strait of Georgia. *Videnskabelige Meddelelser fra Dansk Naturhistorisk Forening* 91: 241–346.

- O’Hara T.D., Stöhr S., Hugall A.F., Thuy B. & Martynov A. 2018. Morphological diagnoses of higher taxa in Ophiuroidea (Echinodermata) in support of a new classification. *European Journal of Taxonomy* 416: 1–35. <https://doi.org/10.5852/ejt.2018.416>
- Oksanen J., Simpson G., Blanchet F., Kindt R., Legendre P., Minchin P., O’Hara R., Solymos P., Stevens M., Szoecs E., Wagner H., Barbour M., Bedward M., Bolker B., Borcard D., Carvalho G., Chirico M., De Caceres M., Durand S., ... Weedon J. 2022. Vegan: Community Ecology Package. R package version 2.6–4. Available from <https://CRAN-R-project.org/package=vegan> [accessed 1 Jul. 2023].
- Padial J.M., Miralles A., de la Riva I. & Vences M. 2010. The integrative future of taxonomy. *Frontiers in Zoology* 7: 16. <https://doi.org/10.1186/1742-9994-7-16>
- Palumbi S. 1996. Nucleic acids II: polymerase chain reaction. In: Hillis D., Moritz C. & Mable B. (eds) *Molecular Systematics*: 205–247. Sinauer Associates, Sunderland.
- Pineda-Enríquez T., Solís-Marín F.A., Hooker Y. & Laguarda-Figueras A. 2013. *Ophioderma peruana*, a new species of brittlestar (Echinodermata, Ophiuroidea, Ophiodermatidae) from the Peruvian coast. *ZooKeys* 357: 53–65. <https://doi.org/10.3897/zookeys.357.6176>
- R Core Team. 2023. R: A language and environment for statistical computing. R Foundation for Statistical Computing, Vienna, Australia.
- Ronquist F., Teslenko M., Mark P.v.d., Ayres D.L., Darling A., Höhna S., Larget B., Liu L., Suchard M.A. & Huelsenbeck J.P. 2012. MrBayes 3.2: Efficient Bayesian phylogenetic inference and model choice across a large model space. *Systematic Biology* 61 (3): 539–542. <https://doi.org/10.1093/sysbio/sys029>
- Solís-Marín F.A., Alvarado J.J., Abreu-Pérez M., Aguilera O., Alió J., Bacallado-Aránega J.J., Barraza E., Benavides-Serrato M., Benítez-Villalobos F., Betancourt-Fernández L., Borges M., Brandt M., Brogger M.I., Borrero-Pérez G.H., Buitrón-Sánchez B.E., Campos L.S., Cantera J., Clemente S., Cohen-Renjifo M., ... Williams S.M. 2013. Appendix. In: Alvarado J.J. & Solís-Marín F.A. (eds) *Echinoderm Research and Diversity in Latin America*: 543–658. Springer-Verlag, Berlin. <https://doi.org/10.1007/978-3-642-20051-9>
- Steinbeck J. & Ricketts E.F. 1941. *Sea of Cortez. A Leisurely Journal of Travel and Research*. Viking Press, New York.
- Stöhr S., O’Hara T.D. & Thuy B. 2012. Global diversity of brittle stars (Echinodermata: Ophiuroidea). *PLoS ONE* 7 (3): e31940. <https://doi.org/10.1371/journal.pone.0031940>
- Stöhr S., Weber A.A.-T., Boissin E. & Chenuil A. 2020. Resolving the *Ophioderma longicauda* (Echinodermata: Ophiuroidea) cryptic species complex: five sisters, three of them new. *European Journal of Taxonomy* 600: 1–37. <https://doi.org/10.5852/ejt.2020.600>
- Stöhr S., O’Hara T. & Thuy B. (eds) 2023a. World Ophiuroidea Database. *Ophioderma teres* var. *unicolor* H.L. Clark, 1940. Available from <https://www.marinespecies.org/Ophiuroidea/aphia.php?p=taxdetails&id=836072> [accessed 11 Jan. 2023].
- Stöhr S., O’Hara T. & Thuy B. (eds) 2023b. World Ophiuroidea Database. *World Register of Marine Species*. Available from <http://www.marinespecies.org/ophiuroidea> [accessed 11 Jan. 2023]. <https://doi.org/10.14284/358>
- Tamura K., Stecher G. & Kumar S. 2021. MEGA11: Molecular Evolutionary Genetics Analysis version 11. *Molecular Biology and Evolution* 38: 3022–3027. <https://doi.org/10.1093/molbev/msab120>

Thuy B. & Stöhr S. 2016. A new morphological phylogeny of the Ophiuroidea (Echinodermata) accords with molecular evidence and renders microfossils accessible for cladistics. *PLoS ONE* 11 (5): e0156140. <https://doi.org/10.1371/journal.pone.0156140>

Varela-Sánchez A., Templado J. & Machordom A. 2020. Aproximación morfológica y molecular al conocimiento de las ofiuras (Echinodermata: Ophiuroidea) en el Parque Nacional Marino Las Baulas (Pacífico Norte, Costa Rica). *Revista de Biología Tropical* 68 (3): 803–817. <https://doi.org/10.15517/RBT.V68I3.39283>

Zhang J., Kapli P., Pavlidis P. & Stamatakis A. 2013. A general species delimitation method with applications to phylogenetic placements. *Bioinformatics* 29 (22): 2869–2876. <https://doi.org/10.1093/bioinformatics/btt499>

Ziesenhenné F.C. 1955. A review of the genus *Ophioderma* Müller and Troschel. In: Allan Hancock Foundation for Scientific Research (eds) *Essays in the Natural Sciences in Honor of Captain Allan Hancock*: 185–201. University of Southern California Press, Los Angeles. <https://doi.org/10.5962/bhl.title.608>

Manuscript received: 4 December 2023

Manuscript accepted: 24 April 2024

Published on: 6 August 2024

Topic editor: Magalie Castelin

Section editor: Didier VandenSpiegel

Desk editor: Pepe Fernández

Printed versions of all papers are deposited in the libraries of four of the institutes that are members of the EJT consortium: Muséum national d'Histoire naturelle, Paris, France; Meise Botanic Garden, Belgium; Royal Museum for Central Africa, Tervuren, Belgium; Royal Belgian Institute of Natural Sciences, Brussels, Belgium. The other members of the consortium are: Natural History Museum of Denmark, Copenhagen, Denmark; Naturalis Biodiversity Center, Leiden, the Netherlands; Museo Nacional de Ciencias Naturales-CSIC, Madrid, Spain; Leibniz Institute for the Analysis of Biodiversity Change, Bonn – Hamburg, Germany; National Museum of the Czech Republic, Prague, Czech Republic; The Steinhardt Museum of Natural History, Tel Aviv, Israël.

Supplementary material

Supp. file 1. Additional non-type material examined of *Ophioderma aija* sp. nov., *Ophioderma bichi* sp. nov., *Ophioderma teres* (Lyman, 1860), and *Ophioderma unicolor* H.L. Clark, 1940 stat. nov. <https://doi.org/10.5852/ejt.2024.947.2625.12053>

Supp. file 2. Comparative type material examined of the eastern Pacific *Ophioderma* Müller & Troschel, 1840. <https://doi.org/10.5852/ejt.2024.947.2625.12055>

Supp. file 3. Methodological specifications and illustrated account of the morphometric measurements and counts obtained for species of *Ophioderma* Müller & Troschel, 1840. **A.** Dorsal disc. **B.** Dorsal view. **C.** Proximal most arm section. **D.** Median arm section. The numbers indicate the arm segments from which the dorsal arm plate pieces and arm spines were counted. **E.** Close-up of the mouth. **F.** Close up

of a jaw. **G.** Proximalmost ventral arm plates. **H.** Median ventral arm plates. Abbreviations: 1VAP_L = first ventral arm plate length; 1VAP_W = first ventral arm plate width; AL = arm length; DD = disc diameter; JawL = jaw length; LOPas = lateral oral papillae; OSh_L = oral shield length; OSh_W = oral shield width; TS_L = adradial tentacle scale length; VAP_L_med = ventral arm plate length (median arm section); VAP_pores = pores between proximalmost ventral arm plates; VAP_W_med = ventral arm plate width (median arm section). <https://doi.org/10.5852/ejt.2024.947.2625.12057>

Supp. file 4. Raw morphometric data. <https://doi.org/10.5852/ejt.2024.947.2625.12059>

Supp. file 5. Accession numbers and data of specimens of *Ophioderma* Müller & Troschel, 1840 included in the DNA analyses. <https://doi.org/10.5852/ejt.2024.947.2625.12061>

Supp. file 6. Results of morphometric analysis (PERMANOVA pairwise comparisons and SIMPER). <https://doi.org/10.5852/ejt.2024.947.2625.12063>

Supp. file 7. Species delimitation hypotheses obtained with the Bayesian Poisson tree processes (bPTP) model based on COI and 16S sequences of *Ophioderma* Müller & Troschel, 1840 (highest Bayesian-supported solution). Blue color indicates those taxa most likely representing different species, and red, individuals of the same species. Numbers on branches indicate posterior probabilities. Sequences obtained in this study are indicated in bold (see [Supp. file 5](#)). <https://doi.org/10.5852/ejt.2024.947.2625.12065>